Université du Québec à Chicoutimi
Département des Sciences Appliquées

Évaluation par réseau de neurones artificiels de l'effet de givrage et de vent sur les lignes de transmission

Par Abdeslam Jamali

Mémoire présenté à l’Université du Québec à Chicoutimi en vue de l’obtention du grade de Maitre ès sciences appliquées (M. Sc. A.) en ingénierie

Jury :

Ahmed Rahem, Ph. D., Professeur, Université du Québec à Chicoutimi, Directeur de recherche

Reda Snaiki, Ph. D., Professeur, École de technologie supérieure à Montréal, Codirecteur de recherche

Reza Jafari Aminabadi, Ph. D., Professeur, Université du Québec à Chicoutimi, Membre interne

Sara Séguin, Ph. D., Professeure, Université du Québec à Chicoutimi, Membre interne

Québec, Canada

RÉSUMÉ

Dans les régions nordiques, les tempêtes hivernales provoquent d'importantes accumulations de glace sur les lignes de transmission, constituant l'une des principales causes de pannes de courant. Ces phénomènes entraînent également des pertes économiques majeures et posent des risques considérables pour les infrastructures et la sécurité publique. Ce mémoire vise à mettre en lumière l'originalité de l'approche proposée, qui repose sur l'utilisation de réseaux de neurones artificiels pour prédire l'effet combiné de l'accumulation de glace et du vent sur les lignes électriques. Présenté sous forme de mémoire par articles, ce travail compile les méthodes et résultats obtenus, publiés dans deux articles scientifiques de journaux. **Le premier article** : il introduit un réseau de neurones à propagation avant (FFNN) conçu pour prédire le rapport glace-liquide (ILR) à partir des données environnementales du Système d'Observation de Surface Automatisé (ASOS). Ce modèle a été optimisé grâce à plusieurs algorithmes métaheuristiques, notamment l'optimisation par essaim de particules (PSO), l'optimiseur de loup gris (GWO), l'algorithme d'optimisation des baleines (WOA) et l'optimiseur de moisissure visqueuse (SMO). Une analyse de sensibilité, basée sur l'indice de Sobol via une expansion en chaos polynomial, a permis d'identifier les paramètres environnementaux les plus influents sur l'ILR : précipitations, température, température du point de rosée et vitesse du vent. Ce modèle optimisé s'est avéré supérieur à l'algorithme de descente de gradient stochastique (SGD). Une fois l'ILR prédit, l'épaisseur de glace peut être calculée en le multipliant par la profondeur des précipitations liquides. **Le deuxième article** : il se concentre sur la cartographie des risques liés à l'accumulation de glace, en exploitant des données de mesures directes provenant du réseau de glacimètres d'Hydro-Québec. Les épaisseurs maximales annuelles de glace sont ajustées à des distributions de probabilité pour estimer les valeurs de retour sur 10, 30 et 50 ans. Ces données ont ensuite été interpolées en utilisant deux techniques : la pondération inverse de la distance (IDWI) et le krigeage ordinaire (OK), permettant de comparer l'efficacité de ces méthodes. En parallèle, les risques de galop sont évalués en appliquant le cadre d'ingénierie des glaces basé sur la performance (PBIE), produisant ainsi des cartes de risque de galop pour différentes périodes de retour. Ces deux articles ont abouti au développement d'un modèle de prédiction précis de l'épaisseur de glace, ainsi qu'au développement de cartes de risques d'accumulation de glace et de galop. Ces outils offrent des évaluations fiables pour une gestion optimisée des infrastructures au Québec, tout en atténuant les impacts des conditions climatiques extrêmes.

ABSTRACT

In northern regions, winter storms cause significant ice accumulation on transmission lines, which is one of the leading causes of power outages. These events also result in substantial economic losses and pose serious risks to infrastructure and public safety. This thesis aims to emphasize the originality of the proposed approach, which involves the use of artificial neural networks to predict the combined effects of ice accumulation and wind on power lines. Presented as a thesis by articles, this work compiles the methods and results obtained, published in two scientific journal articles. **The first article**: it introduces a feedforward neural network (FFNN) designed to predict the ice-to-liquid ratio (ILR) using environmental data from the Automated Surface Observing System (ASOS). The model was optimized using several metaheuristic algorithms, including Particle Swarm Optimization (PSO), Grey Wolf Optimizer (GWO), Whale Optimization Algorithm (WOA), and Slime Mould Optimizer (SMO). A sensitivity analysis, based on the Sobol index via polynomial chaos expansion, identified the most influential environmental parameters on ILR: precipitation, temperature, dew point temperature, and wind speed. The optimized model demonstrated superior performance compared to the stochastic gradient descent (SGD) algorithm. Once the ILR is predicted, the ice thickness can be calculated by multiplying it by the depth of liquid precipitation. **The second article**: it focuses on mapping risks related to ice accumulation using direct measurement data from Hydro-Québec's network of ice gauges. Maximum annual ice thicknesses were fitted to probability distributions to estimate return values for 10, 30, and 50 years. These values were then interpolated using two techniques: Inverse Distance Weighted Interpolation (IDWI) and Ordinary Kriging (OK), enabling a comparative evaluation of their effectiveness. Additionally, galloping risks were assessed using the performance-based ice engineering (PBIE) framework, resulting in galloping risk maps for different return periods. These two articles contributed to the development of a precise prediction model for ice thickness and the creation of risk maps for ice accumulation and galloping. These tools provide reliable evaluations to support optimized infrastructure management in Québec, while reducing the impacts of extreme weather conditions.

TABLE DES MATIÈRES

LISTE DES TABLEAUX

LISTE DES FIGURES

LISTE DES SYMBOLES

A	Cross-sectional area	m^2
A_G	Vertical galloping amplitude	m
b	Bias	-
C_d	Drag coefficient	-
C_l	lift coefficient	-
C_1	Cognitive component	-
C_2	Social component	-
d_c	Conductor's diameter	m
E	Equivalent elastic modulus	GPa
f	Natural frequency of the conductor	Hz
$F_I(I_T)$	Fitted Gumbel distribution	-
g	Gravitational acceleration	9.81 (m/s^2)
G	Galloping factor	0.75m/s
G	Wind gust speed	kts
H	Static tension	kN
I_T	Ice thickness on an elevated horizontal surface	-
k	Parameter related to the number of galloping loops	-

K_c	Conductor stiffness	-
L	Conductor span length	m
m	Mass per unit length	kg/m
m_s	Mass of the conductor	kg/m
n	Number of training samples	-
p_0	Probability of zero ice accretion	-
P	Hourly liquid precipitation rate	in/h
R	Correlation coefficient	-
R_{eq}	Equivalent radial ice thickness	-
(r_1, r_2)	Random values sampled	-
T	Air temperature	℃
T	Static tension	kN
U	Wind speed	kts
$\vec{v}$	Velocity vector	-
V_c	Critical wind speed	m/s
$\vec{X}$	Position vector	-
$\overrightarrow{X}_{gopt}$	Best global position	-
$\overrightarrow{X}_{\mathrm{lopt}}$	Personal best position	-
y	Actual (true) value	-
ŷ	Predicted value generated by the FFNN model	-

LISTE DES SYMBOLES GRECS

α	Angle of attack	°
α	Learning rate	-
θ_{old}	Current weight or bias	-
ξ	Total system damping	-
ξ_s	Structural damping	-
ξ_a	Aerodynamic damping	-
ρ_0	Density of ice	kg/m^3
Φ	Activation function	
ω_n	Natural angular frequency	rad/s
ω_i	Weight associated with input x_i	-

LISTE DES ABRÉVIATIONS

ASOS	Automated Surface Observing System
DPT	Dew Point Temperature
FFNN	Feedforward Neural Network
FRAM	Freezing Rain Accumulation Model
GDP	Generalized Pareto Distribution
GEV	Generalized Extreme Value

GWO	Grey Wolf Optimizer
IDWI	Inverse-Distance Weighted Interpolation
ILR	Ice-to-Liquid Ratio
K-S	Kolmogorov-Smirnov
MC	Monte-Carlo
ML	Machine learning
MSE	Mean Square Error
NCEI	National Centers for Environmental Information
OMP	Orthogonal Matching Pursuit
PBIE	Performance-Based Ice Engineering
PCE	Polynomial Chaos Expansion
PDF	Probability Density Function
PSO	Particle Swarm Optimization
ReLU	Rectified Linear Unit
SGD	Stochastic Gradient Descent
SMO	Slime Mold Optimizer
SVM	Support Vector Machine
STD	Standard Deviation
WOA	Whale Optimizer Algorithm

DÉDICACE

Je dédie ce présent travail à la mémoire précieuse de mes parents, qu'Allah, dans sa miséricorde infinie, les accueille au sein de son paradis.
À ma grande famille, pilier de mon existence, et à ma petite famille, source de mon inspiration et de mon bonheur, je témoigne ma gratitude et mon amour profond.

REMERCIEMENTS

Je tiens tout d'abord à exprimer ma profonde gratitude envers l'Université du Québec à Chicoutimi (UQAC), qui m'a offert l'opportunité d'explorer ce sujet passionnant, riche en enseignements, découvertes et apprentissages.

Je souhaite remercier chaleureusement mon directeur de recherche, Monsieur Ahmed Rahem, ing., Ph. D., ainsi que mon codirecteur de recherche, Monsieur Reda Snaiki, ing., Ph. D., pour leur supervision éclairée, leur encadrement bienveillant, leurs précieux conseils et leur disponibilité sans faille tout au long de ce projet de recherche.

Je tiens également à exprimer ma sincère reconnaissance à Monsieur Éric Morissette, ingénieur chez Hydro-Québec, pour son aide précieuse dans l'obtention des données d'Hydro-Québec, qui ont été essentielles à la réalisation de ce projet.

Enfin, je souhaite adresser mes remerciements les plus chaleureux à tous mes amis pour leur soutien constant et inconditionnel tout au long de mon parcours académique.

CHAPITRE 1

INTRODUCTION GÉNÉRALE

1.1 Introduction

Les aléas météorologiques extrêmes ont toujours représenté des menaces majeures pour notre environnement. Leur intensité et leur fréquence accrues entraînent des répercussions importantes sur notre vie quotidienne, avec des impacts souvent insoutenables, voire catastrophiques. Parmi ces événements, on peut citer les cyclones, les tornades, ainsi que les tempêtes de givre et de verglas, qui se distinguent par leur capacité à perturber de manière significative les écosystèmes et les infrastructures. Ces phénomènes affectent à la fois les éléments naturels et les structures humaines, causant des dommages considérables.

Certaines régions, comme le Canada, la Norvège, la Sibérie, la France et la Chine, sont particulièrement vulnérables aux tempêtes de givre et de verglas. Ces phénomènes se manifestent principalement par l'accumulation de glace sur des infrastructures telles que les lignes de transmission d’énergie (Figure 1.1), les pylônes et les éoliennes, qui deviennent particulièrement fragiles face à ces aléas. La présence de vents aggrave encore les dommages, augmentant la probabilité de ruptures massives des infrastructures.

Un exemple marquant de ces impacts est la tempête de verglas de 1998, qui a frappé l’Ontario et le Québec. Cet événement a provoqué l’effondrement de nombreuses tours de transmission électrique, causant des pertes économiques estimées à près de 1,7 milliard de dollars ((Chang et al., 2007) ; (Chang et al., 2012)). Aussi, en 1998, une autre tempête de verglas survenue entre le 4 et le 10 janvier, a lourdement paralysé Montréal et la région de

Saint-Laurent, privant 1,4 million de personnes d'électricité. Cet événement a entraîné la destruction de 1000 pylônes et l'endommagement de 3000 km de lignes électriques, nécessitant des travaux de reconstruction évalués à 6,4 milliards de dollars (Solangi, 2018). La province du Québec, particulièrement vulnérable aux tempêtes hivernales, subit régulièrement des impacts majeurs liés à ces événements. Les tempêtes de givre perturbent non seulement la distribution d'électricité, mais également la circulation, tout en générant des coûts de réparation très élevés. En effet, le Québec compte 140 000 km de lignes aériennes et des infrastructures critiques régulièrement affectées par ces conditions extrêmes, engendrant d'importants défis économiques et opérationnels (Rajaonarivelo, 2008). Une autre tempête de verglas majeure a touché l'est du Canada en 2013, entraînant des pertes assurées de 200 millions de dollars et des coupures de courant prolongées pour plus d'un million de foyers ((Armenakis & Nirupama, 2014) ; (Sheng et al., 2023)).

En plus de dommages mécaniques remarquables, on peut s'ajouter l'impact psychologique significatif sur les populations vivant dans les zones touchées par ces événements climatiques extrêmes.

Cette étude s'articule autour de deux axes principaux :

1. **Déterminer l'épaisseur de givre** susceptible de se former sur les structures lors d'événements de verglas en s'appuyant sur des modèles fiables.
2. **Évaluer les risques liés à la formation de givre**, particulièrement en présence de vents pouvant déclencher des phénomènes d'instabilité tels que le galop. Une cartographie précise des zones à risque est essentielle pour concevoir des structures adaptées et réduire les risques de ruptures majeures.

Ces objectifs visent à améliorer la compréhension des impacts des tempêtes de givre et à proposer des solutions pour minimiser leurs effets sur les infrastructures et les populations.

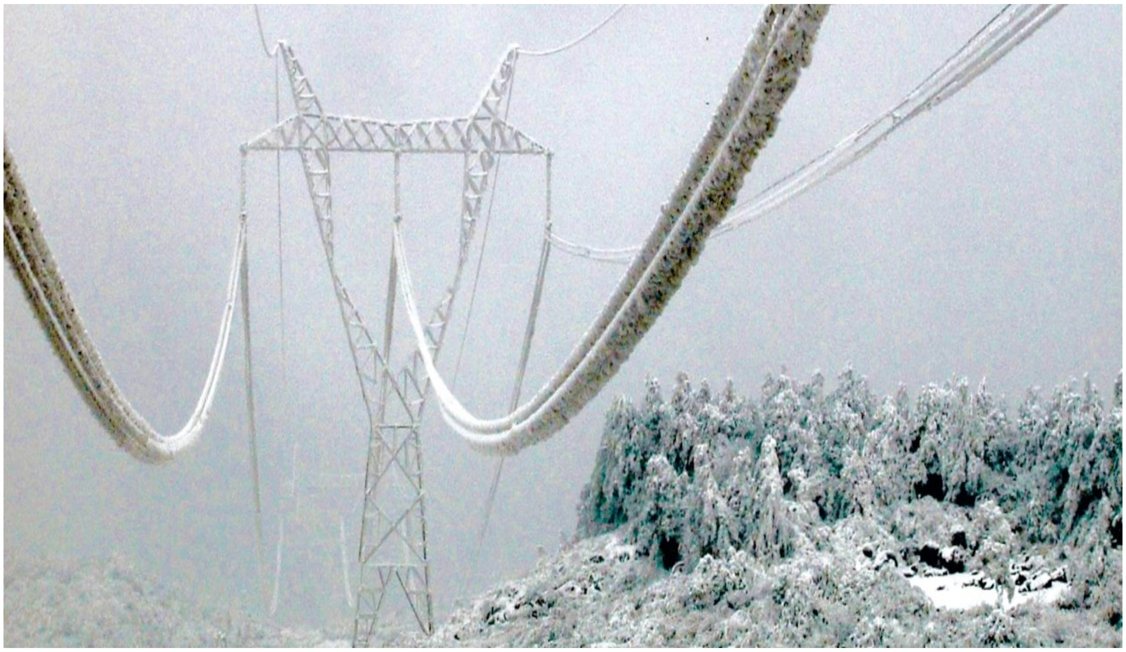

Figure 1.1 *Accumulation du verglas sur les lignes de transmission électriques(Enriching Technical Knowledge of T&D Professionals, 2024)*

1.2 Problématique

Dans le domaine du transport d'électricité, la performance et la fiabilité des lignes de transmission sont essentielles pour assurer une stabilité et une continuité optimales. Cependant, ces infrastructures sont souvent exposées à des conditions climatiques difficiles, comme le givrage et le vent, qui peuvent non seulement compromettre leur fonctionnement, mais aussi poser des risques importants pour leur intégrité structurelle. Afin de répondre à ces défis, il est crucial de concevoir des stratégies et des solutions adaptées pour prévenir ou atténuer les effets néfastes de ces phénomènes. Une compréhension approfondie de leurs mécanismes est donc indispensable pour renforcer la résilience des infrastructures électriques et garantir un approvisionnement énergétique fiable, même dans des conditions extrêmes.

Cette étude met en évidence trois problématiques principales :

1. Effet du givrage sur les conducteurs électriques

Le givrage des conducteurs électriques entraîne la formation d'une couche de glace autour des câbles, augmentant leur poids et affaiblissant leurs composants. Cette surcharge expose les lignes de transmission à un risque accru de défaillances, compromettant ainsi leur fiabilité et pouvant causer des interruptions de service significatives.

L'un des grands défis est de développer un modèle prédictif capable d'estimer efficacement l'épaisseur de glace accumulée lors d'épisodes de verglas. Toutefois, de nombreux modèles existants présentent des limites, telles que :

- Hypothèses simplificatrices dans les modèles mathématiques, qui ne reflètent pas toujours la réalité des phénomènes climatiques.
- Incapacité à intégrer les non-linéarités du système dans les modèles autorégressifs simplifiés.

Pour relever ce défi, cette étude propose le développement d'un modèle fiable, capable de surmonter ces limitations tout en améliorant la précision des prédictions d'épaisseur de glace.

2. Cartographie précise des épaisseurs maximales de glace

Une deuxième problématique concerne la localisation précise des épaisseurs maximales annuelles de glace pour différentes périodes de retour sur la province de Québec. Actuellement, certaines cartes sont établies à partir de données collectées auprès de stations dispersées à travers le Canada, et les calculs des épaisseurs maximales annuelles de glace reposent sur des modèles mathématiques, tels que le modèle de Jones ou d'autres. Cependant, ces approches manquent de précision lorsqu'il s'agit de représenter des zones spécifiques.

Cette étude utilise les données collectées par le réseau de glacimètres d'Hydro-Québec pour surmonter cette lacune. Ces données réelles permettent de :

- Établir des cartes de haute précision des épaisseurs maximales de glace pour des périodes de retour déterminées.
- Améliorer les décisions de conception et d'intervention, en identifiant avec précision les zones les plus vulnérables.

3. Interaction entre le givrage et le vent : risques de galop

Le troisième défi porte sur les risques accrus lorsque le vent s'ajoute au givrage. Ces deux phénomènes combinés peuvent générer des oscillations dynamiques, connues sous le nom de mouvements de galop, qui augmentent considérablement les risques de ruptures structurelles. Ces ruptures soudaines mettent en péril non seulement les infrastructures, mais aussi la continuité de la fourniture d'électricité.

Pour résoudre cette problématique, cette étude propose :

- L'évaluation des amplitudes de galop en appliquant un cadre basé sur la performance en ingénierie (PBIE) aux données réelles d'Hydro-Québec.
- La cartographie des risques de galop pour la province de Québec, permettant d'identifier les zones critiques.

En abordant ces trois problématiques, cette étude vise à fournir des outils et des connaissances pour améliorer la résilience des lignes de transmission face aux défis climatiques, tout en garantissant la sécurité et la continuité de l'approvisionnement électrique.

1.3 Objectifs

L'objectif principal de ce projet est d'évaluer l'effet du givrage à l'aide d'un modèle basé sur les réseaux de neurones artificiels, ainsi que l'effet combiné du givrage et du vent sur les lignes de transmission, en recourant à une technique spécifique.

Pour atteindre cet objectif général, les objectifs spécifiques suivants ont été définis :

1. Développer un modèle à ordre réduit permettant une prédiction rapide de l’évolution temporelle du givre sur une ligne électrique. Ce modèle repose sur deux étapes clés : d’abord, une analyse de sensibilité réalisée à l’aide de la méthode du chaos polynômial en expansion (PCE) ; ensuite, l’utilisation d’un modèle de réseau neuronal à propagation avant (FFNN) optimisé par quatre métaheuristiques (PSO, GWO, WOA et SMO);

2. Élaborer une carte de givrage pour le Québec destinée à la conception, en appliquant une méthode appropriée d’interpolation spatiale. Cette carte sera établie à partir des valeurs correspondant à différentes périodes de retour, déterminées à l’aide d’un modèle probabiliste basé sur la distribution de probabilité de Gumbel;

3. Développer des cartes des risques liés au galop (faible, modéré et élevé) pour le Québec, en ciblant les lignes électriques exposées aux conditions combinées de givre et de vent. Ces cartes seront établies pour différentes périodes de retour, en appliquant le nouveau cadre (PBIE).

1.4 Méthodologie

1.4.1 Modèle de prédiction du ratio glace-liquide (ILR)

Dans l'article présenté au CHAPITRE 2, un nouveau modèle a été développé pour prédire rapidement l'évolution temporelle du ratio glace-liquide (ILR) horaire, un paramètre essentiel pour évaluer l'efficacité de l'accumulation de glace. Ce modèle repose sur un réseau neuronal à propagation avant (FFNN), optimisé à l'aide de techniques avancées telles que l'optimisation par essaims particulaires et d'autres approches métaheuristiques. Les données environnementales utilisées pour cette méthodologie proviennent du Système Automatisé d'Observation de Surface (ASOS). Une analyse de sensibilité globale, basée sur les indices de Sobol calculés à l'aide de l'expansion en chaos polynomial, a permis d'identifier les paramètres d'entrée les plus influents, facilitant ainsi la réduction de la dimensionnalité des variables d'entrée du modèle.

1.4.2 Cartes de conception du givre pour le Québec

Dans le même cadre, l'article du CHAPITRE 3 présente une autre approche, celle de la création de cartes de conception du givre pour le Québec, correspondant à différentes périodes de retour. La méthodologie utilisée pour élaborer ces cartes comprend plusieurs étapes : la collecte de données historiques sur le givre, enregistrées par les stations de glaciomètres entre 1975 et 2020 ; la détermination du modèle probabiliste le mieux adapté aux données, à l'aide de trois distributions de probabilités ; l'estimation des périodes de retour grâce à ce modèle probabiliste ; et enfin, l'application de la technique d'interpolation la plus appropriée pour générer les cartes correspondantes.

1.4.3 Cartes des risques de galop au Québec

Toujours dans le cadre du chapitre 3, une autre série de cartes a été générée, cette fois pour évaluer les risques de galop, en utilisant les résultats obtenus précédemment. Cette approche repose sur l'application du cadre (PBIE), qui optimise la conception des structures de génie civil en produisant des cartes de risque de galop pour différentes périodes de retour. Le cadre PBIE est utilisé pour analyser le risque induit par le galop vertical des conducteurs glacés. Pour modéliser la réponse dynamique des lignes de transmission sous l'effet des charges combinées de vent et de verglas, une approche semi-empirique simplifiée est utilisée, permettant d'estimer l'amplitude du galop, conformément aux travaux de((Lu & Chan, 2009) ; (Lu & Chakrabarti, 2023)).

Ces méthodologies combinées offrent une représentation fiable des risques associés à l'accumulation de glace et au galop. Elles permettent non seulement une meilleure gestion des infrastructures de lignes de transmission, mais aussi une amélioration de la précision des cartes de risque. Grâce à ces outils, cette étude renforce la fiabilité des évaluations pour les infrastructures au Québec, en fournissant des données essentielles pour optimiser leur conception et leur gestion.

1.5 Revue de la littérature

La revue de littérature de cette étude aborde trois aspects principaux : la modélisation de l'accumulation de givre sur les lignes électriques, l'élaboration de cartes de givre et Phénomène du galop des lignes électriques givrées.

1.5.1 Modélisation de l'accumulation de givre sur les lignes électriques

Dans la littérature, divers modèles ont été développés pour estimer l'épaisseur de glace sur les systèmes de lignes de transmission, en prenant en compte des paramètres météorologiques et environnementaux (Lozowski & Makkonen, 2005) .Ces modèles se classent généralement en deux catégories : les modèles basés sur la physique et les modèles basés sur les données (He et al., 2021). Les modèles physiques simulent l'accrétion de glace en s'appuyant sur des processus physiques bien établis, tels que la transmission de chaleur et la mécanique des fluides, intégrés à des formulations mathématiques simplifiées. Ces formulations sont souvent calibrées ou validées à l'aide de données expérimentales, comme l'ont montré plusieurs études ((Imai, 1953); (Lenhard Jr., 1955); (Goodwin et al., 1983); (Makkonen, 1984); (Makkonen, 1998);(Zhang, et al., 2012)).Cependant, l'accrétion de glace étant un phénomène complexe et non linéaire, influencé par de nombreux facteurs environnementaux et marqué par des incertitudes significatives, il est extrêmement difficile de formuler des équations mathématiques capables de simuler ce processus avec précision (He et al., 2021).À l'inverse, les modèles basés sur les données s'appuient sur des informations issues de diverses sources, telles que des relevés sur le terrain et des expériences contrôlées((Saviz Naeini & Snaiki, 2024) ; (Saviz Naeini & Snaiki, 2024)). Ces modèles sont élaborés à l'aide de différentes techniques d'apprentissage automatique, allant de méthodes statistiques simples, comme la régression linéaire((Chaîné & Castonguay, 1974);

(Jones, 1998); (Sanders & Barjenbruch, 2016)) à des algorithmes complexes comme les réseaux de neurones profonds (Wu & Snaiki, 2022).Les formules autorégressives simplifiées, grâce à leur simplicité et leur efficacité computationnelle, ont été largement adoptées dans diverses applications d'ingénierie, notamment pour la production de cartes de givre((Jeong et al., 2018); (Jarrett et al., 2019); (Jeong et al., 2019); (Sheng et al., 2023)). Cependant, leur dépendance à des fonctions de base prédéfinies limite leur capacité à représenter fidèlement des systèmes dynamiques complexes tels que l'accrétion de glace. Face à ces limites, les approches d'apprentissage automatique émergent comme des solutions puissantes pour prédire l'accrétion de glace de manière rapide et précise ((Shabani et al., 2022); (Snaiki, 2024)). Elles peuvent simuler des systèmes dynamiques non linéaires sans se baser sur des hypothèses simplifiées ou une linéarisation. Par exemple, des réseaux de neurones artificiels, entraînés par l'algorithme de rétropropagation, ont été conçus pour modéliser ce processus complexe((Li et al., 2011); (Huang & Li, 2012); (Chen et al., 2012)). En outre, des techniques avancées, telles que les algorithmes génétiques (Du et al., 2010), l'algorithme de colonie de fourmis continue (Yin et al., 2012), et l'algorithme d'optimisation par mouche des fruits (Niu et al., 2017) ont été appliquées pour renforcer les performances de ces réseaux. Les Machines à Vecteurs de Support (SVM) ont également été largement employées dans diverses variantes pour estimer l'épaisseur de glace à partir de paramètres environnementaux((Zarnani et al., 2012); (Dai et al., 2013); (Huang et al., 2014); (Ying & Su, 2014); (Xu et al., 2015); (Ma & Niu , 2016); (Ma et al., 2016); (Niu et al., 2017)). Par ailleurs, des modèles novateurs, comme les machines à apprentissage extrême (Sun & Wang, 2019) et les modèles d'apprentissage profond (He et al., 2021) ont démontré leur efficacité pour cette tâche spécifique. Cependant, malgré le développement de nombreux modèles d'apprentissage automatique (ML) dans ce domaine, une analyse approfondie visant à sélectionner les paramètres environnementaux les plus pertinents parmi un large éventail de variables fait encore défaut. Cette absence de sélection rigoureuse des caractéristiques clés peut entraîner des résultats de simulation imprécis. De plus, la majorité de ces modèles ont été élaborés à partir de scénarios spécifiques, tels que des processus de givrage ou des configurations de lignes de transmission particulières. Ils ne tiennent souvent pas compte de la variabilité des conditions environnementales ou de l'utilisation de grands ensembles de données couvrant des régions géographiquement diversifiées, limitant ainsi leur capacité à généraliser efficacement les prédictions.

1.5.2 Élaboration de cartes de givre

Dans le Code Canadien de Conception des Ponts Routiers (CCCPR) (Association canadienne de normalisation 2019) (Association., 2006), l'épaisseur nominale d'accrétion de glace est définie en fonction de la période de retour de 50 ans correspondant à l'épaisseur maximale annuelle d'accrétion. Les valeurs proposées s'appliquent à quatre régions du Canada, classées selon l'intensité du phénomène : légère, modérée, forte et extrême. Ces épaisseurs nominales sont respectivement de 4, 12, 31 et 66 mm. Selon les commentaires du CCCPR, ces valeurs sont établies à partir d'échantillons obtenus à l'aide du modèle proposé par Chaine et Skeates (1974) (Chaîné & Skeates , 1974). Yip (1995) (Yip, 1995) a utilisé une autre version du modèle, développée par Chaine et Castonguay (1974) (Chaîné & Castonguay, 1974) , pour estimer une période de retour de 30 ans concernant la quantité de glace radiale sur une tige de 25 mm de diamètre dans divers sites canadiens. Les résultats montrent que l'épaisseur radiale équivalente est généralement inférieure à 30 mm à une hauteur de 10 m. Cette épaisseur diminue d'est en ouest et du sud au nord. Une fonction empirique décrivant la variation de l'épaisseur de l'accrétion de glace en fonction de la hauteur est également fournie. Yip a également supposé que l'épaisseur maximale annuelle d'accrétion de glace suit une distribution de Gumbel.

Une mise à jour importante de la carte des risques liés à l'accrétion de glace au Canada a été réalisée par Jarrett et al.(2019) (Jarrett et al., 2019). Ces derniers ont élaboré une carte de risque pour une période de retour de 50 ans, représentant la quantité de glace radiale sur une tige de 25 mm de diamètre. Comme dans les travaux de Yip (1995), la distribution de Gumbel a été utilisée pour modéliser l'épaisseur maximale annuelle. Les tendances spatiales identifiées par Jarrett et al. (2019) (Jarrett et al., 2019) sont similaires à celles de Yip (1995), avec des épaisseurs équivalentes maximales généralement inférieures à 30 mm, sauf dans certaines zones côtières de l'est du pays où elles peuvent atteindre 40 mm.

Sheng et al. (2023) et (Sheng et al., 2023) ont mené une analyse de l'accrétion de glace sur des surfaces horizontales, verticales et sur des fils horizontaux au Canada, en utilisant trois modèles empiriques populaires. Ils ont confirmé que le modèle de Chaine (Chaine et Skeates, 1974), utilisé comme référence opérationnelle par Environnement et Changement climatique Canada (ECCC), fournit des estimations conservatrices comparées à celles obtenues avec le modèle de Goodwin et al. (1983) (Goodwin et al., 1983) ou le modèle simple du Cold Regions Research and Engineering Laboratory (CRREL) développé par Jones (1998). Les travaux de Sheng et al. incluent également des cartes de risque pour la vitesse maximale annuelle équivalente du vent et du verglas, établies pour diverses périodes de retour.

Ces résultats soulignent les défis liés au développement de cartes de conception pour le verglas. La rareté des données constitue un obstacle majeur, accentué par le fait que la plupart des modèles sont conçus pour de vastes régions géographiques (comme le Canada) à partir de stations météorologiques souvent très éloignées les unes des autres. Contrairement aux données sur les vitesses du vent, les enregistrements sur l'accrétion de glace sont rarement disponibles dans les archives météorologiques ou historiques. En conséquence, l'estimation du givre repose principalement sur des modèles empiriques, dont la pertinence peut varier selon les régions, ce qui remet parfois en question la validité des résultats obtenus.

1.5.3 Phénomène du galop des lignes électriques givrées

Les lignes de transmission sont affectées par divers types de chargements aérodynamiques instationnaires et les oscillations qui en résultent (Lou et al., 2023). En présence de glace, ces oscillations, notamment celles induites par le vent, peuvent s'intensifier de manière significative. Bien que les vibrations éoliennes et les oscillations de sillage aient un impact sur la performance dynamique des lignes, principalement en provoquant des charges de fatigue, elles se manifestent généralement par des oscillations de faible amplitude. En revanche, le galop se caractérise par des oscillations de grande amplitude et de basse fréquence (0,1 à 1 Hz), résultant des interactions complexes entre le vent et la glace (McComber & Paradis, 1998). Ce phénomène peut entraîner des mouvements oscillatoires importants, susceptibles de causer des dommages structurels graves, contrairement aux vibrations éoliennes ou aux oscillations de sillage, qui induisent des charges plus localisées.

Le pionnier de l'analyse théorique du galop est Den Hartog (Den Hartog, 1932), qui a expliqué le phénomène comme une instabilité aérodynamique pure appliquée à un système à un degré de liberté (SDOF) soumis à une oscillation verticale. Une extension de cette théorie a été proposée par (Nigol & Clarke, 1974), qui ont décrit le galop comme une instabilité aéroélastique, où le mouvement dépend de l'interaction avec des données structurelles (par exemple, effet inertiel, rigidité en torsion, amortissement).

Selon les auteurs, cet événement, nommé galop total, est provoqué par le couplage des mouvements verticaux et de torsion. Ce mécanisme à deux degrés de liberté a été davantage développé par (Yu et al., 1993), qui ont redéfini le phénomène en utilisant un modèle à trois degrés de liberté en translation et un degré de liberté en torsion. (Liu et al., 2021) ont ajouté une charge d'excitation externe à l'équation régissant les lignes de transmission glacées en se basant sur la condition de vent stable, établissant ainsi un nouveau modèle de vibration auto-excitée forcée pour le galop. (Liu et al., 2021) ont analysé l'exactitude des solutions approximatives obtenues par la méthode de perturbation pour les équations de galop. Sur la base de ces investigations, des critères de conception théorique utiles pour restreindre ou éliminer le galop des lignes de transmission ont été proposés.

D'innombrables tentatives ont été réalisées pour simuler le processus de galop des lignes de transmission en utilisant des méthodes numériques. Sur la base de la théorie des poutres courbées spatiales. (Yan et al., 2013) et (Yan et al., 2014) ont établi deux types de modèles de galop pour les conducteurs glacés, à savoir un modèle de poutre courbée finie et un modèle mixte, afin de simuler le galop des lignes de transmission. En conséquence, une formule pour la vitesse du vent critique a été proposée. (Wu et al., 2018) ont utilisé le logiciel FLUENT pour simuler l'écoulement de l'air autour de deux conducteurs en faisceau. Une méthode de simulation numérique pour l'oscillation du sillage a été proposée et validée par des données de tunnel aérodynamique. Les résultats ont montré que, lorsque le galop se produit, la trajectoire d'un sous-conducteur est proche de l'ellipse horizontale. (Meynen et al., 2005) ont simulé numériquement les caractéristiques d'entrée d'énergie d'un conducteur unique en résolvant un problème d'oscillation harmonique simple en régime laminaire bidimensionnel. (Cluni et al., 2008) ont analysé la durée de vie en fatigue d'une ligne de transmission par des simulations numériques en écoulement laminaire et turbulent. (Desai et al., 1995) ont proposé un élément de câble avec un degré de liberté en torsion pour simuler un conducteur glacé. (Xiong et al., 2011) ont réalisé une analyse modale sur des conducteurs glacés et ont déterminé leur performance en matière de galop en utilisant un modèle de poutre courbée tridimensionnelle. (Zhang et al., 2020) ont effectué un essai aérodynamique sur quatre conducteurs en faisceau et ont analysé les modes de vibration en considérant différents types d'isolateurs. Sur la base de ces investigations, le processus de galop des lignes de transmission peut être reproduit numériquement. Les interactions entre le vent et les lignes de transmission ont été discutées. Cependant, en raison de la complexité et des lacunes en termes de précision et d'efficacité des calculs, leur application à l'ingénierie pratique a été limitée.

Pour étudier les influences de différents facteurs (tels que la vitesse du vent, l'angle d'attaque, la forme de la couverture de glace, etc.) sur le galop, des expériences en souffleries sont réalisées sur des modèles rigides et aéroélastiques. Par exemple (Guo et al., 2019) et (Guo et al., 2020) ont mené une étude expérimentale sur les caractéristiques de galop des conducteurs recouverts de glace. Basée sur le coefficient aérodynamique obtenu par des tests de mesure de force en soufflerie, la proximité entre les résultats de la formule théorique et les résultats expérimentaux a été révélée. Une nouvelle méthode pour protéger les conducteurs recouverts de glace contre le galop a été proposée. ((Chabart & Lilien, 1998); (Zdero & Turan, 2010); (Li et al., 2017); (Lou et al., 2019); (Lou et al., 2020) et (Zhou et al., 2016)) ont réalisé des tests en soufflerie avec des modèles de conducteurs glacés en faisceau unique ou multifaisceaux (quatre, six ou huit conducteurs) soutenus par des ressorts. Ces investigations ont enrichi la compréhension du mécanisme de galop des lignes de transmission, ce qui est précieux pour la prévention et le contrôle du galop. Cependant, dans la plupart des études en souffleries existantes, un ou quelques unités de conducteurs recouverts de glace sont adoptées comme objet de recherche, et les influences de la direction du vent sur les caractéristiques du galop sont rarement prises en compte.

Il convient de noter que le comportement dynamique du système produit par le galop n'est pas pris en compte par les directives de la norme internationale pour la conception des lignes électriques aériennes (IEC 60826:2003) (Commission Électrotechnique Internationale, 2003) (Commission, 2003). Dans cette norme, une épaisseur radiale équivalente pour l'accrétion de glace atmosphérique est supposée, ce qui se réfère à un profil stable et limite l'analyse à une condition statique.

1.6 Structure du Mémoire

Deux articles de revue sont issus de ce mémoire et sont présentés séparément dans les chapitres 2 et 3. La structure générale de ces articles comprend le résumé, l'introduction, la méthodologie, la discussion et la conclusion.

Le chapitre 1 porte sur une introduction générale du projet ainsi que sur la problématique de cette étude. Par la suite, les objectifs spécifiques et généraux sont définis, et la méthodologie du travail ainsi que la revue de littérature sont expliquées.

Le chapitre 2 présente l'article 1, qui traite d'un réseau de neurones basé sur l'optimisation métaheuristique pour la prévision du givrage sur les lignes de transmission.

Le chapitre 3 contient le manuscrit de l'article 2, portant sur le développement de cartes précises du risque de givrage et de galop pour le Québec, grâce à une approche basée sur les données.

Enfin, le chapitre 4 présente les conclusions et les recommandations pour des travaux futurs.

1.7 Références

Chang, S., McDaniels, T., Mikawoz, J., & Peterson, K. (2007). Infrastructure failure interdependencies in extreme events: power outage consequences in the 1998 Ice Storm. *Natural Hazards, 41*, 337–358.

He, L., Luo, J., & Zhou, X. (2021). A Novel Deep Learning Model for Transmission Line Icing Thickness Prediction. (IEEE, Éd.) 733–738.

Jarrett, P., Yau, K.-H., & Morris, R. (2019). Update of the Reference Ice Thickness Amounts due to Freezing Rain for Canadian Codes and Standards . *Proceedings – Int. Workshop on Atmospheric Icing of Structures* , 23 – 28 .

Lenhard Jr., R. (1955). An Indirect Method for Estimating the Weight of Glaze on Wires. *Bulletin of the American Meteorological Society, 36*(1), 1–5.

Sheng, C., Tang, Q., & Hong, H. (2023). Estimating and Mapping Extreme Ice Accretion Hazard and Load Due to Freezing Rain at Canadian Sites. *International Journal of Disaster Risk Science*, 127–142.

Armenakis, C., & Nirupama, N. (2014). Urban impacts of ice storms: Toronto December 2013. *Natural Hazards, 74*, 1291–1298.

Association., C. S. (2006). Design criteria of overhead transmission lines. Dans *CAN/CSA-C22.3.* Rexdale: Ontario: Canadian Standards Association.

Chabart, O., & Lilien, J. (1998). Galloping of electrical lines in wind tunnel facilities. *Journal of Wind Engineering and Industrial Aerodynamics, ,74-76,*, 967-976.

Chaîné, P., & Castonguay, G. (1974). New approach to radial ice thickness concept applied to bundle-like conductors. *Industrial Meteorology Study,.4. AES Environment Canada,*, pp. 22–.

Chaîné, P., & Skeates , P. (1974). *Ice accretion handbook: Freezing.* Ottawa: Environment Canada.

Chang, S., McDaniels, T., Mikawoz, J., & Peterson, K. (2012). Infrastructure Failure Interdependencies in Extreme Events: The 1998 Ice Storm. *Disaster Risk and Vulnerability: Mitigation Through Mobilizing communities and partnerships*, p.275.

Chen, S., Dai, D., Huang, X., & Sun, M. (2012). Short-Term Prediction for Transmission Lines Icing Based on BP Neural Network. *IEEE*, 1-5.

Cluni, F., Gusella, V., & Gusella, V. (2008). Wind tunnel scale model testing of suspended cables and numerical comparison. *Journal of Wind Engineering and Industrial Aerodynamics, 96*(10-11), 1134-1140.

Commission, I. E.-t. (2003). International Standard Design Criteria of Overhead Transmission Lines (IEC 60826). Geneve.

Dai, D., Huang, X.-T., Dai, Z., Hao, Y., Li, L., & Fu , C. (2013). Regression model for transmission lines icing based on support vector machine. *High Voltage Eng, 39*, 2822–2828.

Den Hartog, J. (1932). Transmission Line Vibration Due to Sleet. *Transactions of the American Institute of Electrical Engineers, 51*, 1074 - 1076.

Desai, Y., Yu, P., Popplewell, N., & Shah, A. (1995). Finite element modelling of transmission line galloping. *Computers & Structures, 57(3)*, 407-420.

Du, X., Zheng, Z., Tan, S., & Wang, J. (2010). The Study on the Prediction Method of Ice Thickness of Transmission Line Based on the Combination of GA and BP Neural Network. *IEEE*, 1-4.

Enriching Technical Knowledge of T&D Professionals. (2024, november 8). (INMR) Consulté le novembre 25, 2024, sur Impact & Mitigation of Icing on Power Network Equipment Utility Practice & Experience. https://www.inmr.com/impact-mitigation-icing-power-network-equipment/

Goodwin, T., Mozer, J., & DiGioia, A. (1983). Predicting ice and snow loads for transmission line design. *Predict. Ice Snow Loads Trans. Line Design*, 267–273.

Guo, P., Li, S., & Li, S. (2020). Analysis of wind attack angle increments in wind tunnel tests for the aerodynamic coefficients of iced hangers. *Advances in Structural Engineering, 23(4)*.

Guo, P., Wang, D., Li, S., Liu, L., & Wang, X. (2019). Transiting test method for galloping of iced conductor using wind generated by a moving vehicle. *Wind and Structures, 28(3)*, 155-170.

He, L., Luo, J., & Zhou, X. (2021). A Novel Deep Learning Model for Transmission Line Icing Thickness Prediction. (IEEE, Éd.) 733–738.

He, L., Luo, J., & Zhou, X. (2021). A Novel Deep Learning Model for Transmission Line Icing Thickness Prediction. (IEEE, Éd.) pp. 733–738.

Huang, X., & Li, J. (2012). Icing thickness prediction model using BP Neural Network. (IEEE, Éd.)

Huang, X., Xu, J., Yang, C., Wang, J., & Xie , J. (2014). Transmission line icing prediction based on data driven algorithm and LS-SVM. *Autom. Electr. Power Sys, 38*, 81–86.

Imai, I. (1953). Studies of ice accretion. *Res. Snow Ice, 1*, 35-44.

Jarrett, P., Yau, K.-H., & Morris, R. (2019). Update of the Reference Ice Thickness Amounts due to Freezing Rain for Canadian Codes and Standards. 23-28.

Jeong, D., Cannon, A., & Zhang, X. (2019). Projected changes to extreme freezing precipitation and design ice loads over North America based on a large ensemble of Canadian regional climate model simulations. *Natural Hazards and Earth System Sciences, 19*, 857–872.

Jeong, D., Sushama, L., Vieira, M., & Koenig, K. (2018). Projected changes to extreme ice loads for overhead transmission lines across Canada. *Sustainable Cities and Society, 39*, 639-649.

Jones, K. (1998). A simple model for freezing rain ice loads. *Atmospheric Research, 46*, 87–97.

Li , X.-m., Nie , X.-c., Zhu , Y.-k., Yi, Y., & Yan , Z.-t. (2017). Wind Tunnel Tests on Aerodynamic Characteristics of Ice-Coated 4-Bundled Conductors. *Mathematical Problems in Engineering*, 11. https://doi.org/628173

Li, P., Li, Q., Cao, M., Gao, S., & Huang, H. (2011). Time series prediction for icing process of overhead power transmission line based on BP neural networks. (IEEE, Éd.) *Proceedings of the 30th Chinese Control Conference*, 5315-5318.

Liu, X., Yang, S., Min, G., Cai, M., Wu, C., & Jiang, Y. (2021). Investigation on the Accuracy of Approximate Solutions Obtained by Perturbation Method for Galloping Equation of Iced Transmission Lines. *Mathematical Problems in Engineering* .

Liu, X., Yang, S., Wu, C., Zou, M., Min, G., Sun, C., & Cai, M. (2021). Planar Nonlinear Galloping of Iced Transmission Lines under Forced Self-Excitation Conditions. *Discrete Dynamics in Nature and Society*.

Lou, W., Huang, C., Huang, M., & Yu, J. (2019). An aerodynamic anti-galloping technique of iced 8-bundled conductors in ultra-high-voltage transmission lines. *Journal of Wind Engineering and Industrial Aerodynamics, 193*. https://doi.org/103972

Lou, W., Wu, D., Xu, H., & Yu, J. (2020). Galloping Stability Criterion for 3-DOF Coupled Motion of an Ice-Accreted Conductor. *ASCE, 146(5)*.

Lou, W.-j., Zhang, Y.-l., Gu, Y., Luo, G., Bai, H., Huang, M.-f., Virk, M., & Bian, R. (2023). An improved rigid rod method for wind-induced swing response prediction of heavily iced transmission lines. *Journal of Wind Engineering and Industrial Aerodynamics, 235*. https://doi.org/105358

Lozowski, E., & Makkonen, L. (2005). Fifty years of progress in modelling the accumulation of atmospheric ice on power network equipment.

Lu, M. L., & Chan, J. K. (2009). A Rational Design Equation for Galloping. *Int. Conference on Ultra-High Voltage Transmission,Beijing, China*.

Lu, M., & Chakrabarti, D. (2023). Design ice and wind on overhead transmission lines in British Columbia. *Cold Regions Science and Technology, 214*. https://doi.org/103960

Ma, T., & Niu , D. (2016). Icing Forecasting of High Voltage Transmission Line Using Weighted Least Square Support Vector Machine with Fireworks Algorithm for Feature Selection. *Applied Sciences, 6*(438).

Ma, T., Niu , D., & Fu, M. (2016). Icing Forecasting for Power Transmission Lines Based on a Wavelet Support Vector Machine Optimized by a Quantum Fireworks Algorithm. *Applied Sciences, 6*(54).

Makkonen, L. (1984). Modeling of Ice Accretion on Wires. *Journal of Applied Meteorology and Climatology, 23*(6), 929–939.

Makkonen, L. (1998). Modeling power line icing in freezing precipitation. *Atmospheric Research, 46*(1–2), 131-142.

McComber, P., & Paradis, A. (1998). A cable galloping model for thin ice accretions. *Atmospheric Research, 46(1-2)*, 13-25.

Meynen, S., Verma, H., Hagedorn, P., & Schäfer, M. (2005). On the numerical simulation of vortex-induced vibrations of oscillating conductors. *Journal of Fluids and Structures, 21(1)*, 41-48.

Nigol, O., & Clarke, G. (1974). Conductor galloping and control based on torsional mechanism. *IEEE Transactions on Power Society*.

Niu, D., Wang , H., Chen, H., & Liang, Y. (2017). The General Regression Neural Network Based on the Fruit Fly Optimization Algorithm and the Data Inconsistency Rate for Transmission Line Icing Prediction. *Energies, 10*(2066).

Niu, D., Wang, H., Chen, H., & Liang, Y. (2017). The General Regression Neural Network Based on the Fruit Fly Optimization Algorithm and the Data Inconsistency Rate for Transmission Line Icing Prediction. *Energies, 10*(2066).

Rajaonarivelo, R. (2008). Intégration Des Données Manquantes. *Maitrise en Inginierie*, 2. Chicoutimi, Département Sciences appliquées,Québec, Canada: Université Du Québec À Chicoutimi.

Sanders, K., & Barjenbruch, B. (2016). Analysis of Ice-to-Liquid Ratios during Freezing Rain and the Development of an Ice Accumulation Model. *Weather and Forecasting, 31*(4), 1041–1060.

Saviz Naeini, S., & Snaiki, R. (2024). A novel hybrid machine learning model for rapid assessment of wave and storm surge responses over an extended coastal region. *Coastal Engineering, 190*(104503), 1-12.

Saviz Naeini, S., & Snaiki, R. (2024). A physics-informed machine learning model for time-dependent wave runup prediction. *Ocean Engineering, 295*(116986), 1-12.

Shabani, M., Jamali, A., Snaiki, R., & Rahem, A. (2022). Prediction of Ice Accretion on Transmission Lines using Hybrid Particle Swarm Optimization-based Artificial Neural Networks.

Sheng, C., Tang, Q., & Hong, H. (2023). Estimating and Mapping Extreme Ice Accretion Hazard and Load Due to Freezing Rain at Canadian Sites. *International Journal of Disaster Risk Science, 14*, 127-142.

Snaiki, R. (2024). Performance-based ice engineering framework: A data-driven multi-scale approach. *Cold Regions Science and Technology, 224*(104247), 1-13.

Solangi, A. R. (2018, June). Icing Effects on Power Lines and Anti-icing and De-icing Methods. *Master*, p:6. Faculty of Science and Technology, Norway: The Arctic University Of Normay UIT.

Sun, W., & Wang, C. (2019). Staged icing forecasting of power transmission lines based on icing cycle and improved extreme learning machine. *Journal of Cleaner Production, 208*, 1384-1392.

Wu, C., Yan, B., Huang, G., Zhang, B., Lv, Z., & Li, Q. (2018). Wake-induced oscillation behaviour of twin bundle conductor transmission lines. *Royal Society Open Science, 5(6)*. https://doi.org/180011

Wu, W., & Snaiki, R. (2022). Applications of Machine Learning to. *Front. Built Environ, 8*(811460), 1-41.

Xiong, H., Li, Z., & Yan, Z. (2011). Modal Analysis of the Iced Transmission Line Based on Three-Dimensional Curved Beam Element. *Advanced Materials Research, 291-294*, 2049-2054.

Xu, X., Niu, D., Wang, P., Lu, Y., & Xia, H. (2015). The Weighted Support Vector Machine Based on Hybrid Swarm Intelligence Optimization for Icing Prediction of Transmission Line. *Mathematical Problems in Engineering*.

Yan, Z., Li, Z., Savory, E., & Lin, W. (2013). Galloping of a single iced conductor based on curved-beam theory. *Journal of Wind Engineering and Industrial Aerodynamics, 123(Part A)*, 77-87.

Yan, Z., Savory, E., Li, Z., & Lin, W. (2014). Galloping of iced quad-conductors bundles based on curved beam theory. *Journal of Sound and Vibration, 333(6)*, 1657-1670.

Yin, S., Lu, Y., Wang, Z., Li, P., & Xu, K. (2012). Icing thickness forecasting of overhead transmission line under rough weather based on CACA-WNN. *Electr. Power Sci. Eng,, 11*.

Ying, Z.-R., & Su, X.-L. (2014). Icing thickness forecasting of transmission line based on particle swarm algorithm to optimize SVM. *J. Electr. Power, 29*, 6-9.

Yip, T.-C. (1995). Estimating icing amounts caused by freezing precipitation in Canada. *Atmospheric Research, 36(3-4)*, 221-232.

Yu, P., Desai, Y., Shah, A., & Popplewell, N. (1993). Three-degree-of-freedom model for galloping. Part I: Formulation. *Journal of Engineering Mechanics, 119*, 2404-2425.

Zarnani, A., Musilek, P., Shi, X., Ke, X., He, H., & Greiner, R. (2012). Learning to predict ice accretion on electric power lines. *Engineering Applications of Artificial Intelligence, 25*(3), 609-617.

Zdero, R., & Turan, O. (2010). The effect of surface strands, angle of attack, and ice accretion on the flow field around electrical power cables. *Journal of Wind Engineering and Industrial Aerodynamics, 98,10-11,*, 672-678.

Zhang, , Z., Huang, , H., Jiang, , X., Hu, , J., & Sun, , C. (2012). Analysis of ice growth on different. *Diangong Jishu Xuebao (Transact. China Electrotech. Soc.), 27*, 35–43.

Zhang, Z., Wang, D., Wang, T., Yu , Z., Huang, Z., & Zhang, D. (2020). Aeroelastic Wind Tunnel Testing on the Wind-Induced Dynamic Reaction Response of Transmission Line. *Journal of Aerospace Engineering, 34(1)*.

Zhou, L., Yan, B., Zhang, L., & Zhou, S. (2016). Study on galloping behavior of iced eight bundle conductor transmission lines. *Journal of Sound and Vibration, 362*, 85-110.

CHAPITRE 2

ARTICLE 1: A METAHEURISTIC-OPTIMIZATION-BASED NEURAL NETWORK FOR ICING PREDICTION ON TRANSMISSION LINES

Reda Snaiki [a*], Abdeslam Jamali [b], Ahmed Rahem [b], Mehdi Shabani [a], Brian L. Barjenbruch [c]

[a] Department of Construction Engineering, École de Technologie Supérieure, University of Quebec, Montreal, QC, Canada

[b] Department of Applied Sciences, Université du Québec à Chicoutimi, Chicoutimi, QC, Canada

[c] NOAA/National Weather Service, Valley, Nebraska, USA

[*]*Corresponding author email*: reda.snaiki@etsmtl.ca

https://doi.org/10.1016/j.coldregions.2024.104249

Submitted to *Cold Regions Science and Technology*.

Received 27 March 2024; Received in revised form 23 May 2024; Accepted 7 June 2024

Available online 8 June 2024

Acknowledgement:

This work was supported by the Natural Sciences and Engineering Research Council of Canada (NSERC) [grant number CRSNG RGPIN 2022-03492].

Authors contribution:

Reda Snaiki: Writing – review & editing, Writing – original draft, Visualization, Validation, Supervision, Software, Resources, Project administration, Methodology, Investigation, Funding acquisition, Formal analysis, Data curation, Conceptualization. **Abdeslam Jamali:** Writing – original draft, Software, Data curation, Methodology. **Ahmed Rahem:** Writing – review & editing, Supervision, Investigation, Formal analysis, Conceptualization. **Mehdi Shabani:** Investigation, Software. **Brian L. Barjenbruch:** Writing – review & editing, Investigation, Formal analysis, Data curation.

Résumé

L'accumulation de glace sur les lignes de transmission aériennes est une des principales causes des pannes d'électricité et peut entraîner des pertes économiques importantes dans les régions nordiques. Il est donc crucial de prédire de manière précise et rapide l'accumulation de glace sur les lignes électriques pour assurer le bon fonctionnement du réseau électrique. Cette étude propose une méthode d'apprentissage automatique pour prédire le ratio glace-liquide (ILR), un paramètre important pour évaluer l'efficacité de l'accumulation de glace. Bien que l'estimation de l'ILR soit essentielle pour les prévisions opérationnelles, de nombreux modèles existants d'accumulation de glace ne prennent pas en compte cette capacité. Un réseau de neurones à propagation avant (FFNN) entraîné avec la méthode de descente de gradient stochastique et divers optimisateurs métaheuristiques - spécifiquement l'optimisation par essaims particulaires, l'optimiseur loup gris, l'optimiseur baleine, et l'optimiseur de moisissure visqueuse - est utilisé pour prévoir l'ILR à l'heure. Les données environnementales nécessaires pour l'entraînement et le test du modèle FFNN ont été obtenues à partir du système automatisé d'observation de surface (ASOS). Une analyse de sensibilité globale utilisant l'indice de Sobol, évalué via les coefficients d'une expansion en chaos polynomial, a été réalisée pour identifier les paramètres d'entrée les plus influents. Les résultats indiquent que seulement quatre paramètres d'entrée contribuent de manière significative à la variance de la réponse : les précipitations, la température, la température du point de rosée et la vitesse du vent. De plus, le modèle FFNN entraîné avec des optimisateurs métaheuristiques a surpassé l'approche par descente de gradient stochastique. Avec l'ILR prédit, l'accumulation de glace peut être facilement calculée comme le produit de l'ILR et de la quantité de précipitations liquides.

Mots-clés : Accumulation de glace ; Ratio glace-liquide ; Apprentissage automatique ; Sélection de caractéristiques ; Optimiseur métaheuristique.

Abstract

Ice accretion on overhead transmission line systems is a leading cause of power outages and can lead to substantial economic losses in northern regions. Therefore, accurately and rapidly predicting ice accretion on power lines is crucial for ensuring the safe operation of the power grid. This study introduces a machine learning method for predicting the ice-to-liquid ratio (ILR), an important parameter for assessing ice accretion efficiency. While estimating ILR is vital for operational forecasting, many existing ice accretion models do not include this capability. A feedforward neural network (FFNN) trained with stochastic gradient descent and various metaheuristic optimizers - specifically particle swarm optimization, grey wolf optimizer, whale optimizer, and slime mold optimizer - is employed to forecast hourly ILR. Environmental data required for training and testing the FFNN model were obtained from the Automated Surface Observing System (ASOS). A global sensitivity analysis using the Sobol index, evaluated via the coefficients of a polynomial chaos expansion, was conducted to identify the most influential input parameters. The results indicate that only four input parameters significantly contribute to the variance in the response: precipitation, temperature, dew point temperature, and wind speed. Furthermore, the FFNN model trained with metaheuristic optimizers outperformed the stochastic gradient descent approach. With the predicted ILR, ice accumulation can be easily calculated as the product of ILR and the amount of liquid precipitation depth.

Keywords: Ice accretion; Ice-to-liquid ratio; Machine learning; Feature selection; Metaheuristic optimizer.

2.1 Introduction

Maintaining grid reliability and safety becomes a significant challenge for utilities operating in regions susceptible to freezing temperatures and winter storms due to ice accretion on transmission lines ((Ruszczak & Tomaszewski, 2014), (Tomaszewski et al., 2019)). This ice buildup can lead to catastrophic events when combined with wind loads, causing power outages, structural damage, and substantial economic losses (Fikke et al., 2008).Furthermore, ice accumulation threatens the integrity of the distribution network, potentially exceeding infrastructure capacity and triggering cascading failures. Understanding the mechanisms of ice load formation is crucial, as it can lead to power line failures through two primary modes: structural overload and galloping. For instance, Ontario and Quebec experienced a major ice storm in 1998 that caused the collapse of several power transmission towers and nearly $1.7 billion in economic losses ((Chang et al., 2007), (Chang et al., 2012)). Similarly, an ice storm in eastern Canada in 2013 resulted in $200 million in insured losses and extended power outages for over 1 million customers((Armenakis & Nirupama, 2014), (Sheng et al., 2023)) . In the US alone, icing events are estimated to inflict an average annual cost of $313 million (Zarnani et al., 2012). With the increasing frequency of extreme weather events due to global warming, severe weather-induced icing incidents have become one of the most significant risks in power grid operations ((Jeong et al., 2019), (Chen et al., 2020)). Therefore, accurate and rapid prediction of icing events and their severity is crucial for assisting impacted communities and electric power companies in preparing for ice events, guiding decision-making processes, designing preventive measures, and planning for recovery (DeGaetano et al., 2008).

Several models have been proposed in the literature to predict ice thickness on transmission lines systems by considering meteorological and environmental parameters (Lozowski & Makkonen, 2005). Generally, these models can be categorized as physics-based or data-driven (He et al., 2021). Physics-based models simulate ice accretion by integrating established physical processes such as heat transmission principles and fluid mechanics with simplified mathematical formulations which might be calibrated or validated using experimental data ((Imai, 1953) , (Lenhard Jr., 1955) , (Makkonen, 1984) , (Makkonen, 1998), (Zhang et al., 2012)). However, since ice accretion is a complex, nonlinear process influenced by several environmental factors with numerous uncertainties, generalizing mathematical equations to accurately simulate this process is extremely challenging (He et al., 2021). On the other hand, data-driven models utilize data from different sources such as field measurements and controlled experiments. These models can then be derived using various machine learning techniques, ranging from relatively simple statistical methods like linear regression ((Chaîné & Castonguay, 1974), (Jones, 1998), (Sanders & Barjenbruch, 2016)) to complex algorithms like deep neural networks (Wu & Snaiki, 2022). The simplicity and computational efficiency of simplified autoregressive formulas have led to their widespread implementation in various engineering applications, such as ice maps generation (((Jeong et al., 2018), (Jarrett et al., 2019), (Jeong et al., 2019), (Sheng et al., 2023)).However, the use of predefined basis functions and autoregressive formulas may not be suitable for accurately modeling such complex dynamic systems. Alternatively, machine learning approaches can be considered as effective tools for rapidly predicting ice accretion ((Shabani et al., 2022), (Snaiki, 2024)). They can simulate nonlinear dynamic systems without relying on simplified assumptions or linearization. For example, artificial neural networks trained using the backpropagation algorithm have been developed for simulating ice accretion ((Li et al., 2011), (Huang & Li, 2012), (Chen et al., 2012)) . Other techniques, such as genetic algorithms (Du et al., 2010), the continuous ant colony algorithm (Yin et al., 2012), and the fruit fly optimization algorithm (Niu et al., 2017) have also been used to enhance neural network performance in ice accretion prediction. Various versions of Support Vector Machine (SVM) models have also been employed to predict ice thickness based on available environmental factors ((Zarnani et al., 2012), (Dai et al., 2013), (Huang et al., 2014), (Ying & Su, 2014), (Xu et al., 2015), (Ma & Niu , 2016), (Ma et al., 2016), (Niu et al., 2017)). Additionally, models like the extreme learning machine (Sun & Wang, 2019) and deep learning models (He et al., 2021) have been developed for ice accretion prediction. While several machine learning (ML) models have been developed for predicting ice accretion, a thorough investigation into feature selection to identify the best environmental parameters for the ML model among multiple variables has been lacking. Failure to select the most influential factors could result in inaccurate simulation results. Additionally, these models have often been developed based on the same icing processes or the same transmission lines, without considering varying environmental conditions or utilizing large, geographically diverse datasets.

Most ML applications have been developed to predict the equivalent radial ice thickness, which is notoriously challenging to measure directly. In addition, in operational weather forecasting, accurately predicting ice accretion thickness remains a challenge due to the inherent variability in icing efficiency (e.g., runoff rate). As a result, various assumptions (e.g., assumed ice accretion efficiency) are often employed to approximate it, introducing significant uncertainties into the prediction process. In contrast, the ice-to-liquid ratio (ILR), which represents the ratio of accumulated ice depth to accumulated liquid depth on a specific surface, is a crucial parameter used to assess the efficiency of ice accretion. By directly targeting ILR, which depends on readily predictable parameters including temperature, wind, and precipitation rate, it is possible to simplify the complex process of assessing icing efficiency and achieve substantially more accurate ice accretion forecasts for upcoming weather events. However, despite the importance of ILR

estimation, particularly for operational forecasting, most existing ice accretion models do not provide this information. Sanders and Barjenbruch (2016) investigated the effects of several environmental factors on ILRs using a large ASOS database. They developed the Freezing Rain Accumulation Model (FRAM), which predicts hourly ILRs based on three environmental factors: wind speed, precipitation rate, and wet-bulb temperature. With the predicted ILR, ice accumulation can be easily calculated by multiplying the ILR by the amount of liquid precipitation accumulation. The resulting ice depth can then be used to estimate ice accretion thickness on elevated objects, whether on a flat surface or as a radial ice thickness measurement, using simplified formulas (Ryerson & Ramsay, 2007). However, it is important to note that FRAM is a simplified autoregressive model and may not capture the nonlinearities within the system accurately.

This study addresses the safety of power transmission/distribution infrastructure by focusing on improved ice accretion prediction on overhead transmission lines. Specifically, the hourly ILR (calculated using the hourly accumulated ice and liquid depths) will be predicted using a feedforward neural network (FFNN) trained with several metaheuristic optimizers. This approach aims to overcome the limitations of gradient-based algorithms, which are known for their relatively slow convergence rates and susceptibility to getting stuck in local minima. Metaheuristics utilize heuristics as informed guesses to guide the search process towards promising regions in the solution space. To accomplish this, the environmental data of freezing rain events over the United States was extracted from the Automated Surface Observing System (ASOS). Six ASOS-observed environmental parameters were selected, representing the mean values calculated over 60-minute duration of continuous freezing rain precipitation. These parameters are air temperature, dew point temperature, sustained wind speed, wind gust speed, precipitation rate, and wet-bulb temperature. A global sensitivity analysis was then conducted to evaluate the impact of each input parameter on the ILR. This analysis utilized Sobol variance decomposition, which was evaluated analytically from the coefficients of a polynomial chaos expansion (PCE) metamodel and compared with the Monte Carlo technique. Additionally, the obtained Sobol's indices were compared with the total Kucherenko indices to further assess their significance. After identifying the most influential input parameters in terms of their variance contribution to the ILR, they will be used as inputs to the FFNN model. This model will be trained using four metaheuristic optimization algorithms: particle swarm optimization (PSO), grey wolf optimizer (GWO), whale optimizer (WOA), and slime mold optimizer (SMO), as well as the stochastic gradient descent approach. The simulation results will then be compared and discussed to evaluate the performance of each optimization method in predicting the ILR. It should be noted that accurate ILR predictions offer significant benefits to grid operators by enabling proactive management strategies. These strategies include pre-emptive de-icing of power lines or load reduction during periods of anticipated heavy ice accumulation, thereby mitigating the risk of line failures. Furthermore, real-time or near real-time ILR predictions enhance situational awareness, allowing grid operators to better anticipate and respond to weather events that could lead to outages. Finally, improved ice load forecasts inform targeted maintenance schedules, focusing resources on areas most susceptible to ice-related damage. This combination of proactive measures, enhanced awareness, and optimized maintenance ultimately contributes to a more resilient power grid infrastructure.

2.2 Feedforward Neural Network

Feedforward neural networks (FFNNs) are supervised neural networks used in a wide range of applications, including regression and classification. These algorithms excel at learning hidden patterns within data and providing dependable predictions. Two well-known architectures of FFNNs are the multi-layer perceptron and deep neural networks. Both consist of an input layer, one or more hidden layers, and an output layer. Each neuron within these layers performs a specific calculation to transform the data it receives. The output of each neuron can be calculated as follows:

$$y = \phi(\sum_{i=1}^{n} \omega_i x_i + b) \tag{1}$$

where ϕ = activation function; ω_i = weight associated with input x_i; and b = bias. The activation function is responsible for capturing the nonlinearities present in the data and can be selected from a range of commonly used functions, such as hyperbolic tangent, sigmoid, ReLU, and others. To train FFNNs, suitable values for the weights and biases need to be determined to establish a desirable relationship between the predicted and expected outputs. This is typically achieved using an optimization algorithm. For example, the backpropagation algorithm is commonly employed to update the weights and biases of FFNNs. It does so by propagating the error (the difference between predicted and expected outputs) backward through the network and adjusting the weights and biases based on the gradient of the error. More specifically, with a predefined loss function E, the new weight or bias (θ_{new}) can be obtained based on the following formula:

$$\theta_{new} = \theta_{old} - \alpha \frac{\partial E}{\partial \theta} \tag{2}$$

where θ_{old} = current weight or bias; and α = learning rate. While the backpropagation technique has been widely used to train neural networks in various applications, it does have certain drawbacks. Specifically, this gradient-based algorithm is known for its relatively slow convergence rate and its susceptibility to getting stuck in local minima. Additionally, the backpropagation technique can suffer from the vanishing and exploding gradient problems, which can significantly affect the training of the neural network. To address these issues, advanced optimization techniques, such as those based on metaheuristic algorithms, have been developed. These techniques aim to overcome the limitations of traditional backpropagation by providing more efficient and robust training methods for neural networks. A schematic representation of a FFNN model trained with a metaheuristic algorithmic is depicted in Figure 2.1.

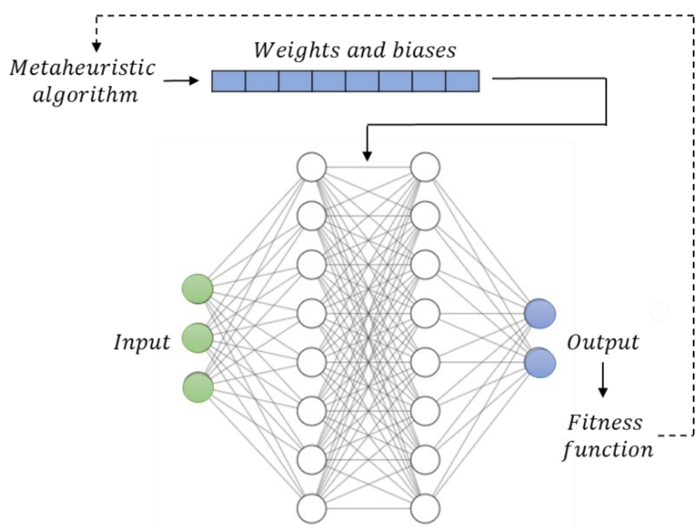

Figure 2.1 *Schematic of a FFNN model trained with a metaheuristic algorithm*

2.3 Metaheuristic Algorithms

A metaheuristic is a procedure that uses nature-inspired heuristics to effectively balance exploration and exploitation strategies, aiming to find an optimal solution. Unlike conventional methods that rely on continuous and differentiable objective functions (such as gradient-based techniques), metaheuristic algorithms have the capability to handle highly nonlinear and non-differentiable problems. Metaheuristic algorithms can be broadly classified into three categories (Ojha et al., 2017): 1. Single solution-based methods which focus on improving a single solution iteratively ((Kirkpatrick et al., 1983); (Mladenovic & Hansen, 1997)); 2. Population-based methods which manage a group of solutions, inspired by natural phenomena like evolution (genetic algorithms) or swarm behaviour (particle swarm optimization) ((Geem et al., 2001); (Rashedi et al., 2009)); 3. Hybrid methods which combine multiple metaheuristic models for enhanced optimization.

In this study, four state-of-the-art population-based algorithms will be employed and compared to optimize the weights and biases of FFNNs, namely the particle swarm optimization (PSO), the grey wolf optimizer (GWO), the whale optimizer (WOA) and the slime mould optimizer (SMA). A brief description of each algorithm will be provided in the following sections.

2.3.1 Particle swarm optimization

Particle Swarm Optimization (PSO) is a population-based optimization algorithm that emulates the behaviour of bird flocks or fish schools. It is suitable for both single-objective and multi-objective optimization problems (Kennedy & Eberhart, 1995). In PSO, a population of potential candidate solutions, referred to as particles, explores a search space to find optimal or near-optimal solutions by iteratively updating their positions. Each particle updates its position by considering its own best-known position as well as the best-known position of the entire swarm. The updated velocity ($\vec{v}^{j+1}$) and position ($\vec{X}^{j+1}$) for each particle are derived based on the current velocity ($\vec{v}^{j}$) and position ($\vec{X}^{j}$) (indicated by j) as:

$$\vec{v}^{j+1} = \vec{v}^{j} + C_1 r_1 . \left[\vec{X}^{j}_{lopt} - \vec{X}^{j}\right] + C_2 r_2 . \left[\vec{X}^{j}_{gopt} - \vec{X}^{j}\right] \tag{3}$$

$$\vec{X}^{j+1} = \vec{X}^{j} + \vec{v}^{j+1} \tag{4}$$

where $\vec{X}$ = position vector; $\vec{v}$= velocity vector; $\vec{X}_{lopt}$ = personal best position; $\vec{X}_{gopt}$ = best global position; C_1 = cognitive component; C_2 = social component; and (r_1, r_2) = random values sampled from an interval $[0,1]$. It should be noted that for the PSO algorithm to effectively identify a global optimal solution, the hyperparameters, including the cognitive and social components, along with the inertia weight, should be carefully selected based on the specific optimization problem. Additionally, the termination criterion is typically linked to a maximum number of iterations or a desired level of solution quality. This careful selection of hyperparameters and termination criteria is crucial for the algorithm to converge efficiently and produce high-quality solutions.

2.3.2 Grey wolf optimizer

The Grey Wolf Optimizer (GWO) is a population-based optimization algorithm inspired by the social leadership and hunting behaviour of grey wolves. This optimization algorithm divides the population into four main groups known as alpha (α), beta (β), delta

(δ), and omega (ω) wolves. The alpha, beta, and delta wolves, representing the three fittest individuals, assume leadership roles and guide the other wolves towards promising regions in the search space. During the optimization process, the wolves update their current positions (indicated by j) around the alpha, beta, or delta wolves using the following equations:

$$\vec{X}^{j+1} = \vec{X_p}^{j} - \vec{A}.\vec{D} \tag{5}$$

$$\vec{D} = \left|\vec{C}.\vec{X_p}^{j} - \vec{X}^{j}\right| \tag{6}$$

where $\overrightarrow{X_p}$ = position of the prey; $\vec{X}$ = position of a grey wolf; and ($\vec{A}, \vec{C}$) = coefficient vectors which help to explore different regions around the best agent in the search space during the optimization process.

Throughout the optimization process, it is assumed that the first three best solutions are represented by α, β and δ, respectively. The remaining wolves (ω) reposition themselves based on α, β and δ. Specifically, the following quantities which determine the distances between the current position and α, β and δ, respectively, are first determined:

$$\overrightarrow{D_\alpha} = \left|\overrightarrow{C_1}.\overrightarrow{X_\alpha} - \vec{X}\right| \qquad \overrightarrow{D_\beta} = \left|\overrightarrow{C_2}.\overrightarrow{X_\beta} - \vec{X}\right| \qquad \overrightarrow{D_\delta} = \left|\overrightarrow{C_3}.\overrightarrow{X_\delta} - \vec{X}\right| \tag{7}$$

where $\overrightarrow{X_k}$ = position of the k wolf (with $k = \alpha$, β or δ); and ($\overrightarrow{C_1}, \overrightarrow{C_2}, \overrightarrow{C_3}$) = random vectors. Then the updated position $\vec{X}^{j+1}$ can be calculated as:

$$\vec{X}^{j+1} = \left[\left(\overrightarrow{X_\alpha} - \overrightarrow{A_1}.\overrightarrow{D_\alpha}\right) + \left(\overrightarrow{X_\beta} - \overrightarrow{A_2}.\overrightarrow{D_\beta}\right) + \left(\overrightarrow{X_\delta} - \overrightarrow{A_3}.\overrightarrow{D_\delta}\right)\right]/3 \tag{8}$$

where ($\overrightarrow{A_1}, \overrightarrow{A_2}, \overrightarrow{A_3}$) = random vectors. It should be noted that the boundary constraints are applied to the new positions to ensure that they remain within the defined problem boundaries. This is important to prevent solutions from going beyond the feasible region of the problem space.

2.3.3 Whale optimizer

The Whale Optimization Algorithm (WOA) is a population-based optimization algorithm that utilizes a population of search agents to iteratively enhance a set of random candidate solutions by emulating the bubble-net feeding behaviour of humpback whales. Its objective is to identify the global optimum for the optimization problem. The search process is divided into two phases: exploration and exploitation. During the exploitation phase, represented by a random coefficient vector $\vec{A}$ where $|\vec{A}| \leq 1$, the next position $\vec{X}^{j+1}$ is determined as follows:

$$\vec{X}^{j+1} = \begin{cases} \overrightarrow{X^*}^{j} - \vec{A}.\vec{D} & if\ p < 0.5 \\ \overrightarrow{D'}.\exp(bl).\cos(2\pi l) + \overrightarrow{X^*}^{j} & if\ p \geq 0.5 \end{cases} \quad (9)$$

where p = a random number in the range $[0,1]$; $\overrightarrow{X^*}$ = position of the best solution; $\vec{D} = \left|\vec{C}.\overrightarrow{X^*}^{j} - \vec{X}^{j}\right|$; $\overrightarrow{D'} = \left|\overrightarrow{X^*}^{j} - \vec{X}^{j}\right|$; $\vec{C}$ = coefficient vector; b = a constant that determines the shape of spiral bubble-net; and l = a random number in the range $[-1,1]$. On the other hand, the exploration phase (represented by a random coefficient vector $|\vec{A}| > 1$) can be formulated as follows:

$$\vec{X}^{j+1} = \vec{X}_{rand} - \vec{A}.\vec{D} \quad (10)$$

where $\vec{X}_{rand}$ = random position vector selected from the current whale optimization; and $\vec{D} = \left|\vec{C}.\vec{X}^{j}_{rand} - \vec{X}^{j}\right|$.

2.3.4 Slime mold optimizer

The Slime mold optimizer (SMO) is a population-based optimization algorithm that emulates the foraging behaviour and morphological transformations observed in slime mold Physarum Polycephalum to explore the search space and find the optimal or near-optimal solutions. This optimizer utilizes weight values to mimic the positive and negative feedback of the bio-oscillator during the foraging stage, resulting in the formation of a diverse feeding vein network thickness, while the slime mold's morphology undergoes changes through three distinct contraction patterns. The algorithm operates in two primary phases: the approach phase, where it searches for food, and the wrap phase, where it exploits the identified food. It iterates between these two phases in an oscillating manner. The mathematical formulation which mimics the slime mold behaviour is given as:

$$\vec{X}^{j+1} = \begin{cases} rnd.(ub - lb) + lb & if\ rnd < z \\ \vec{X}^{j}_{b} + \vec{v_b}.\left(\vec{W}.\vec{X}^{j}_{A} - \vec{X}^{j}_{B}\right) & if\ r < p \\ \vec{v_c}.\vec{X}^{j} & if\ r \geq p \end{cases} \tag{11}$$

where $(\vec{X}_A, \vec{X}_B)$ = two randomly selected individuals from the population; $\vec{X}_b$ = location of the individual with the optimal fitness; $\vec{W}$ = weight of the slime mold; $\vec{v_b}$ = a parameter within the range of $[-a, a]$; $\vec{v_c}$ = a parameter which decreases linearly from one to zero; lb and ub are the lower and upper boundaries of the search range; p = a selected value controlling the exploration and exploitation processes; (rnd, r) = random values in the range of $[0,1]$; and z = a hyperparameter that controls the balance between exploration and exploitation. It's worth noting that the first term of the equation signifies the random exploration process, where the hyperparameter z can be selected based on the specific problem being studied. The second and third terms correspond to the exploration and exploitation phases, respectively.

2.3.5 Metaheuristic design for training FFNNs

Metaheuristic algorithms are suitable for various applications, including those related to Feedforward Neural Networks (FFNNs), due to their capability to provide near-optimal solutions for complex and non-differentiable problems. These algorithms can be utilized to optimize different aspects of FFNNs, such as weights and biases, architecture, activation functions, and other hyperparameters like learning rate. However, they have been primarily employed to optimize weights and biases for fixed architectures, aiming to minimize the overall error of FFNNs.

In this study, the four selected metaheuristic models, namely PSO, GWO, WOA, and SMO, are employed to train a FFNN with a single hidden layer. To achieve this, the weights and biases of a candidate neural network are first stored in a one-dimensional vector, with the vector's length corresponding to the total number of weights and biases in the FFNN. Next, an objective function (or fitness function) is defined for the metaheuristic algorithm, aiming to optimize the FFNN's ability to achieve the highest accuracy in either regression or classification applications. In this study, the mean square error (MSE) metric is chosen as the fitness function for the four metaheuristic algorithms and can be expressed as:

$$MSE = \frac{1}{n}\sum_{i-1}^{n}(y - \hat{y})^2 \qquad (12)$$

where y = actual (true) value; $\hat{y}$ = predicted value generated by the FFNN model; and n = number of training samples. It should be noted that the correlation coefficient R will also be employed to assess the performance of the proposed model. The proposed procedure is illustrated in Figure 2.2.

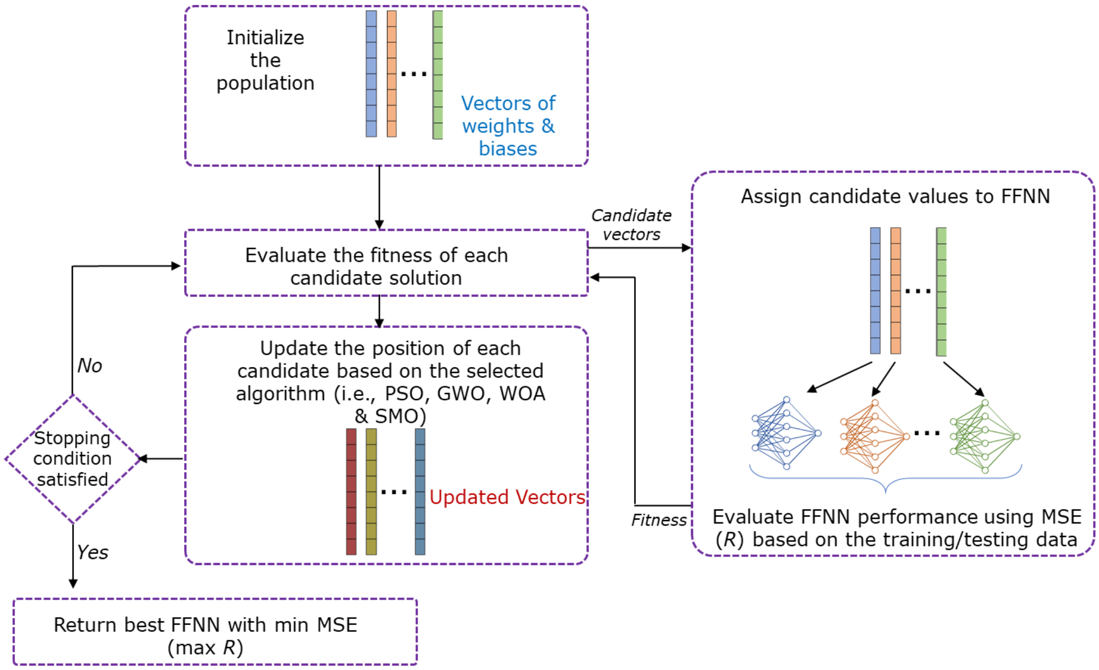

Figure 2.2 *General steps of the metaheuristic-based FFNN model*

2.4 Application

In this section, four selected metaheuristic algorithms, namely PSO, GWO, WOA, and SMO, will be employed to train a feedforward neural network (FFNN). The objective is to predict the ice-to-liquid ratio, which in turn determines the thickness of ice accretion on overhead transmission lines. This section will start will the ice accretion problem and datasets, followed by a discussion of feature selection. Finally, the training and testing results will be presented, along with an analysis and discussion of the findings.

2.4.1 Ice accretion problem & datasets

Ice accretion on overhead lines refers to the gradual buildup of ice on conductors, insulators, or other components of power transmission systems due to freezing precipitation. This accumulation can lead to failure due to the weight of the ice accretion, especially when combined with additional physical stress applied when the lines are exposed to wind, potentially resulting in power outages and even the collapse of the power transmission system. Therefore, accurate and rapid prediction of ice accretion on transmission lines is vital for ensuring system reliability, public safety, preventing power disruptions, and planning resource allocation for improved recovery time. In this study, a FFNN is proposed to rapidly predict the ice-to-liquid ratio (ILR) which can then be used to predict ice accretion on elevated surfaces including power lines.

The data used to train the neural networks were obtained from the Automated Surface Observing System (ASOS). ASOS is an advanced network of meteorological instruments and sensors operated by various agencies, including the National Weather Service. It collects real-time weather data such as wind speed and direction, temperature, atmospheric pressure, and precipitation. By analyzing ASOS data during freezing precipitation events, it is possible to accurately measure ice accretion on elevated surfaces. These ice accretion measurements are observed at the same time and location as the additional atmospheric variables, making it possible to correlate atmospheric conditions to ILR. For this study, ice accumulation data was acquired from the National Centers for Environmental Information (NCEI) for the period 2013-2017, encompassing 407 ASOS sites and providing geographically diverse coverage (Sanders & Barjenbruch, 2016). The data consisted of 60-minute periods with continuous freezing rain, resulting in 2646 observations. To isolate impactful freezing rain events, further filtering criteria were applied. Events were excluded if they lacked any 60-minute period with precipitation rates exceeding 0.50 mm/h (0.02 in/h) or ice accumulation rates below 0.25 mm/h (0.01 in/h), as these events were unlikely to cause significant infrastructure issues. Finally, a meticulous manual quality control process ensured data integrity by eliminating periods with missing or unreasonable meteorological data required for calculating mean sustained wind speed or wet-bulb temperature. This rigorous filtering resulted in a final dataset of 1355 high-quality observations. Six environmental parameters were evaluated as potential predictors of the ILR, with the mean of each parameter calculated over the 60-minute duration of continuous freezing rain precipitation. These parameters are the air temperature (T[℃]), dewpoint temperature (DPT[℃]), sustained wind speed (U[kts]), wind gust speed (G[kts]), hourly liquid precipitation rate (P[in/h]), and wet-bulb temperature (WBT[℃]). To ensure data quality, rigorous quality control procedures were implemented to remove any invalid or physically implausible data points.

It is important to highlight that the proposed ML model aims to predict ILR, a key parameter for operational forecasting. Directly targeting ILR, which depends on readily predictable parameters (e.g., temperature, wind, and precipitation rate), can help overcome the challenges associated with varying icing efficiency. This approach offers the potential for significantly more accurate ice accretion forecasts for upcoming weather events compared to directly predicting ice accretion thickness, which is challenging due to its inherent variability in icing efficiency. The ILR represents the ratio between the accumulated depth of ice on a specific surface and the accumulated depth of liquid, which, by definition, occurs on a horizontal surface. Given the ILR, the ice thickness on an elevated horizontal surface I_T can be obtained using the following formula (Sanders & Barjenbruch, 2016):

$$I_T = \sum_0^h ILR \times P \quad (13)$$

where h = number of hours over which the precipitation occurs. The equivalent radial ice thickness on an elevated surface (R_{eq}) can be then obtained using the following empirical formula (Ryerson & Ramsay, 2007):

$$R_{eq} = 0.394 I_T \quad (14)$$

2.4.2 Input selection

In order to select the best input variables for the FFNN model, this study employs the Sobol index. The Sobol index assesses the portion of the output variance that can be attributed to each input variable or combination of variables. The first-order Sobol's index quantifies the individual effect of each input variable on the output variability by measuring the proportion of the total variance that can be attributed to a specific input variable independently of other variables. On the other hand, higher-order Sobol's indices quantify the combined effects of two or more variables on the output, measuring the extent to which interactions contribute to the total output variance. Similarly, the total Sobol index quantifies the proportion of the total output variance that can be attributed to a particular variable, considering all possible interactions with the other variables.

To calculate Sobol's indices, the study employs an analytical approach based on the coefficients of a polynomial chaos expansion (PCE) metamodel, which is constructed using ASOS data. This involves characterizing random inputs and constructing the PCE to enable the computation of Sobol's indices. Each uncertain model parameter is represented by a random variable and a corresponding probability density function (PDF) in the form $X \sim f_X(x)$. The selection of appropriate probability distributions for the environmental parameters involved a two-step process. First, visual inspection of data histograms and knowledge of the physical characteristics of each parameter guided the identification of candidate distributions. The Kolmogorov-Smirnov (K-S) test then served as a final step to assess the goodness-of-fit between the candidate distributions and the empirical distributions observed in the dataset. This approach ensured that the chosen distributions closely resembled the actual data, enhancing the model's accuracy.

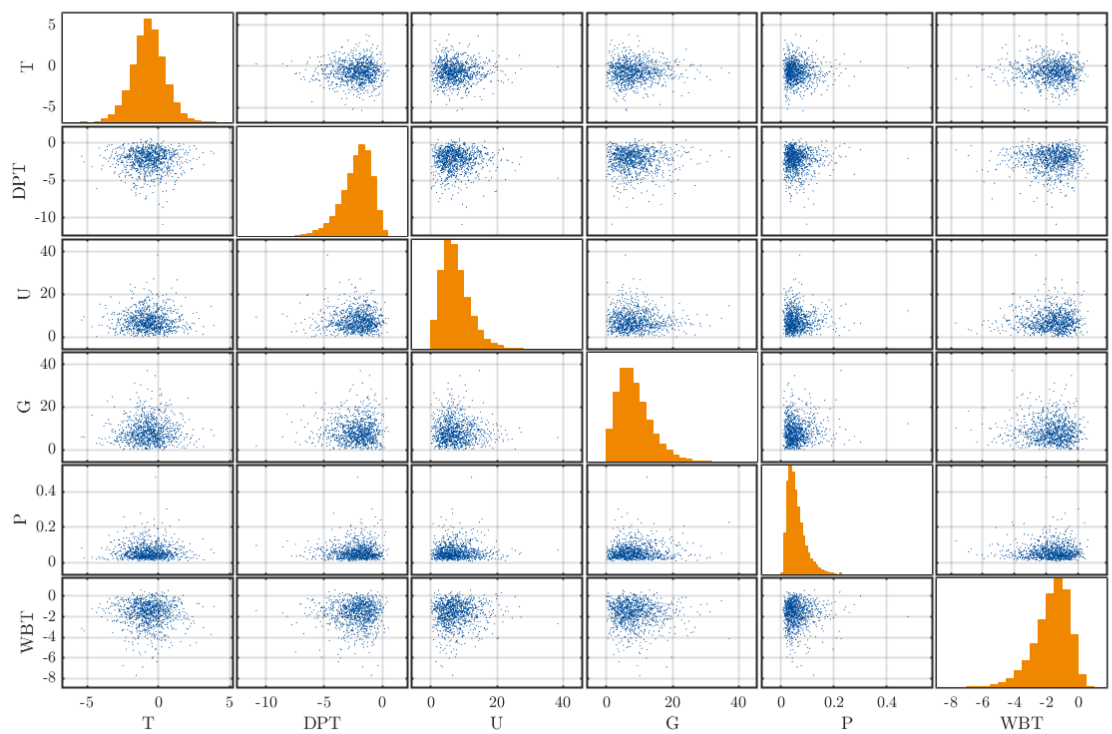

***Figure 2.3** Drawing samples from the obtained marginal PDF corresponding to the environmental parameters*

The histograms in the figure represent the marginal distributions for each variable, while the plots in the lower/upper diagonals depict the sampled points from the bidimensional histograms. The distributions found for the variables are as follows: a logistic distribution for T, Gumbel Min for DPT, Gumbel for U, Gumbel for G, lognormal for P, and Gumbel Min for WBT. It is important to note that the Gumbel distribution refers to the maximum Gumbel distribution or the extreme value distribution of type I, while Gumbel Min corresponds to the Gumbel minimum extreme value distribution, also known as the Smallest Extreme Value (Type I) distribution. For the obtained marginal distributions, a custom set of polynomials that are orthonormal to the non-standard distribution is used in this study. Specifically, the univariate orthonormal polynomials are computed numerically using the *Stieltjes* procedure (Stieltjes, 1884). Given these univariate orthonormal polynomials, a total-degree truncation scheme is defined, which includes all polynomials in the given input variables of a total degree less than or equal to the specified maximum polynomial degree p (in this case, $p = 12$). To compute the PCE coefficients, a sparse PCE method called Orthogonal Matching Pursuit (OMP) ((Pati et al., 1993), (Mallat & Zhang, 1993)) is employed. The global sensitivity analysis is conducted using the PCE-based technique and compared to the Monte-Carlo-based technique, as shown in Figure 2.4.

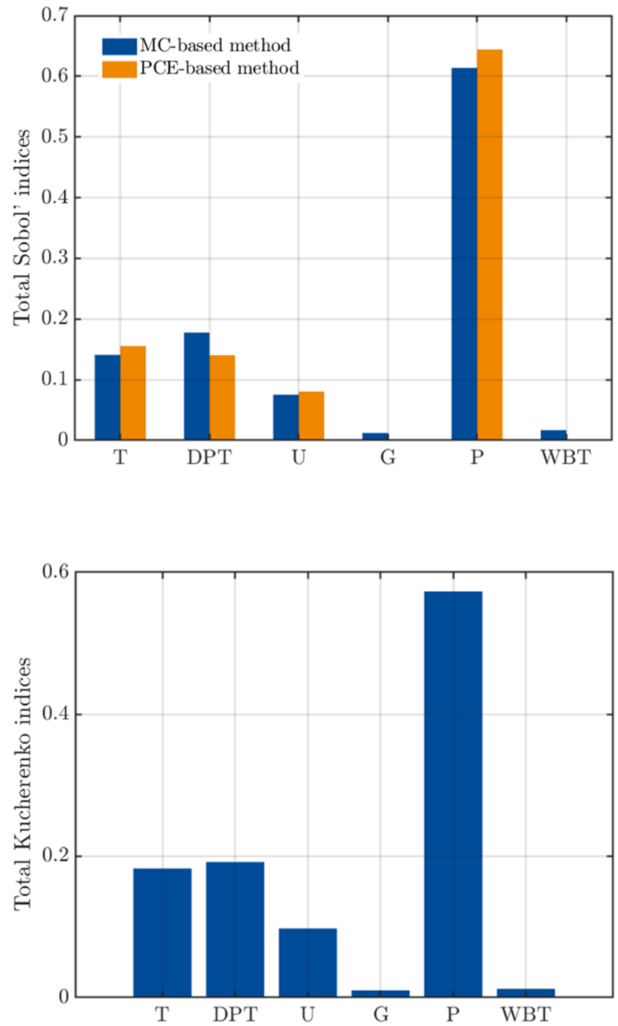

Figure 2.4 *Total Sobol indices evaluated using the MC and PCE approaches (left) and total Kucherenko indices (right)*

The results indicate that only four stochastic dimensions significantly contribute to the response's variance. Precipitation (P), mean temperature (T), dew point temperature (DPT), and mean wind speed (U) are the most dominant environmental factors, with precipitation having the most significant effect on ice accretion. As a result, gust wind (G) and wet-bulb temperature (WBT) will be excluded from subsequent simulations, and only the four dominant environmental factors will be used as inputs for the FFNN model. Furthermore, the results from the Monte Carlo technique closely align with those from the

PCE-based technique. To validate the findings, the total Kucherenko indices are also depicted in Figure 2.4, providing additional insight into dependent input variables and supporting similar conclusions. It is worth noting that while wet bulb temperature is generally considered an important factor in predicting precipitation type, the data used in this study specifically focused on freezing rain events and did not show a significant relationship with this predictor. While not a primary objective of this study, an inclusion of non-freezing rain events (where the ILR is 0) could reveal a more prominent role for wet bulb temperature as a predictor.

2.4.3 Results and discussion

The architecture of the selected FFNN model includes: 1. An input layer comprising the mean air temperature (T), mean dewpoint temperature (DPT), mean sustained wind speed (U), and precipitation rate (P); 2. One hidden layer containing 21 neurons, determined through trial and error; and 3. An output layer with a single variable representing the ice-to-liquid ratio (ILR) as shown in Figure 2.5. The selected activation function for the hidden layer is ReLU, while a linear activation function is chosen for the output layer. Before training, all input datasets are normalized using the min-max normalization technique. Seventy percent of the data is randomly assigned to the training set, with the remaining thirty percent reserved for testing.

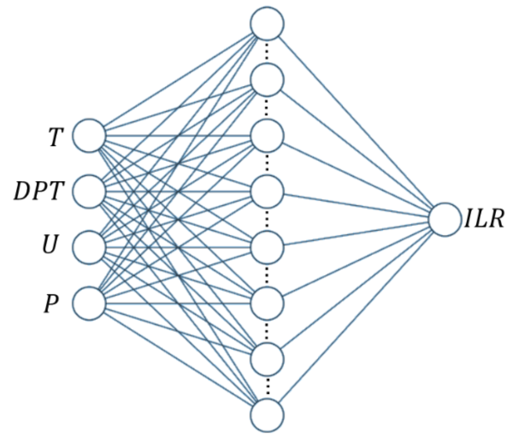

Figure 2.5 *FFNN architecture*

The FFNN model was trained using the four selected metaheuristic models—PSO, GWO, WOA, and SMO—following the approach outlined in Sect. 2.3. Additionally, ten different runs were executed for each metaheuristic algorithm to statistically characterize the results. A population size of 70 was chosen for all four metaheuristic models, determined through a trial-and-error approach. The convergence curves for all metaheuristic optimizers, depicting MSE over 200 iterations for a single independent run, are shown in Figure 2.6. The figure illustrates that all selected metaheuristic optimizers exhibit good optimization efficiency and fast convergence, typically requiring fewer than 50 iterations. Furthermore, GWO demonstrates the fastest convergence speed for the ice accretion dataset.

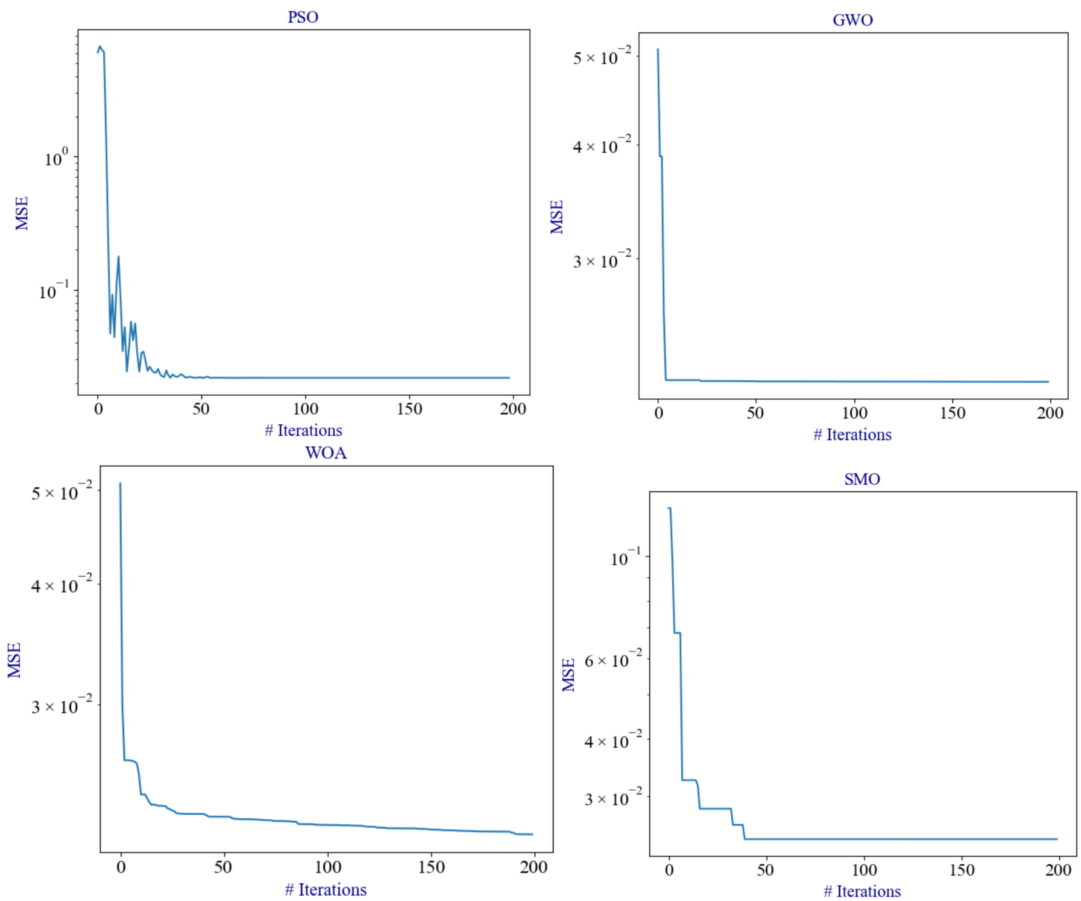

Figure 2.6 *MSE convergence curves using the PSO, GWO, WOA and SMO optimizers*

To evaluate the performance of the metaheuristic optimizers, they were compared against the standard stochastic gradient descent (SGD) algorithm. Table 2.1 presents the average, median, standard deviation (STD), and best MSE across all training samples from ten independent runs.

***Table 2.1**. Average, median, standard deviation, and best of MSE for all training samples over 10 independent runs using several optimization algorithms*

Algorithm	Average MSE	Median MSE	STD MSE	Best MSE
SGD	4.30E-02	4.24E-02	3.12E-03	3.91E-02
PSO	2.19E-02	2.19E-02	9.94E-05	2.17E-02
GWO	2.24E-02	2.22E-02	5.22E-04	2.19E-02
WOA	2.21E-02	2.21E-02	1.32E-04	2.19E-02
SMO	2.42E-02	2.44E-02	5.40E-04	2.31E-02

From Table 2.1, it is evident that FFNN models trained using metaheuristic algorithms outperform the model trained with stochastic gradient descent in terms of average, median, and standard deviation of MSE. This indicates their superior ability to avoid local minima in this context. Among the metaheuristic optimizers, PSO, WOA, and GWO stand out with average MSE values of 2.19E-02, 2.21E-02 and 2.24E-02, respectively. Additionally, all four metaheuristic models exhibit low standard deviation, suggesting robustness and stability compared to SGD. Figure 2.7 displays Boxplots for 10 runs of SGD, PSO, GWO, WOA, and SMO. The Boxplots provide a clear view of the optimizer variability in terms of MSE values across all runs. These plots further confirm the superior performance of metaheuristic optimizers over the classical SGD algorithm. Notably, WOA and PSO demonstrate the best performance, followed by GWO, as evidenced by their low average MSE values and compact boxes, indicating the stability of the proposed training algorithms.

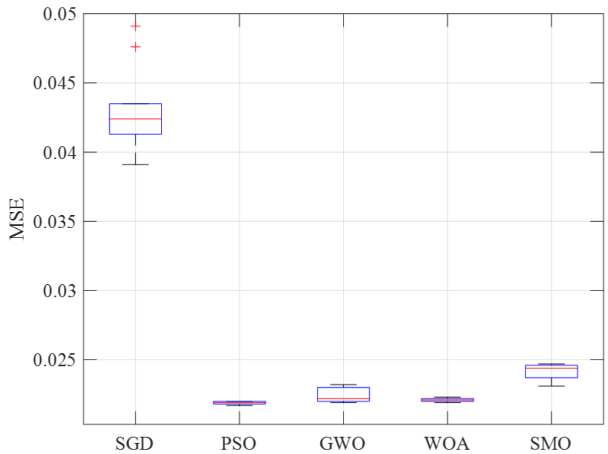

Figure 2.7 *Boxplot representation of the MSE for SGD, PSO, GWO, WOA and SMO on the ice accretion dataset*

Table 2.2 summarizes the MSE and correlation coefficient (*R*) achieved by the different models on the testing set. PSO, GWO, and WOA displayed superior performance, consistent with the training set observations. Notably, these algorithms achieved comparable MSE values (around 2.29E-02) and high correlation coefficients (above 0.80).

Table 2.2*. Mean square error (MSE) and correlation coefficient (R) of the test set using several optimization algorithms.*

	Algorithm				
	SGD	PSO	GWO	WOA	SMO
MSE	4.98E-02	2.29E-02	2.29E-02	2.29E-02	2.57E-02
R	0.58	0.81	0.80	0.81	0.79

Based on this comparative study, it can be concluded that the metaheuristic optimizers outperformed the standard gradient descent approach. Compared to SGD, heuristic optimization algorithms offer several advantages that contribute to their superior performance in this study. SGD's reliance on gradient descent can lead it to get trapped in local optima, while heuristic optimizers excel at balancing exploration and exploitation. This exploration ability potentially helps them escape shallow local minima and find better solutions. Additionally, SGD performance is highly sensitive to learning rate selection, whereas heuristic algorithms typically require less hyperparameter tuning and can identify suitable configurations more efficiently. Finally, real-world problems often have complex error surfaces with multiple local minima. In essence, heuristic optimization's ability to balance exploration and exploitation, combined with less sensitivity to hyperparameter tuning, empowers it to navigate complex error surfaces and potentially outperform SGD in this specific application.

The performance of the proposed metaheuristic approach is further evaluated on 20 randomly chosen icing events from the testing set. These events' ILRs are predicted using both the metaheuristic optimizers and the standard SGD technique. The resulting predictions are then compared against the actual ASOS-based ILR values. Figure 2.8 visualizes these comparisons.

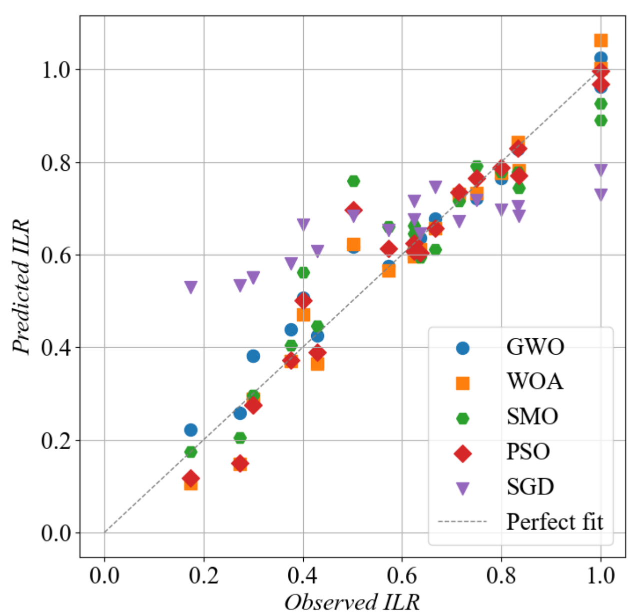

Figure 2.8 *Comparison of observed (ASOS) and predicted hourly ILR for 20 randomly selected icing events using metaheuristic and SGD optimization technique*

Examination of the figure reveals that the metaheuristic approach generally outperforms the SGD technique. This is evident by the closer proximity of most points to the perfect-fit line ($y = x$) for the metaheuristic results. Additionally, the SGD model exhibits a tendency to overestimate ILRs below 0.65 and underestimate them for higher values.

To comprehensively understand the influence of various environmental parameters on the predictive performance of the neural network models, a systematic investigation was conducted. The initial step involved optimizing the neural network while incorporating all six initial environmental parameters. Subsequently, the performance of various four-parameter combinations was explored. Finally, a three-parameter model was tested using the three parameters most commonly employed in similar studies. The model trained with all six input parameters achieved comparable results in terms of prediction accuracy. However, this approach came at the expense of significantly increased training time. This rise in training time can be attributed to the model's increased complexity, requiring a more intricate optimization process with a larger number of tuning parameters. Next, the performance of various combinations of four input parameters was investigated. This analysis revealed that certain combinations, particularly those that included the core set identified by the Sobol index analysis (detailed in Table 2.3), achieved acceptable results. The best MSE values obtained during ten independent training runs for each combination are reported in Table 2.3. Finally, the three-parameter model incorporating the most commonly used parameters exhibited acceptable performance. However, the four-parameter set identified through the Sobol index analysis consistently yielded the best overall results. This four-parameter model achieved a superior balance between prediction accuracy and training efficiency. These findings strongly support the effectiveness of the global sensitivity analysis (Sobol index) in accurately identifying the most influential combination of input parameters for this specific neural network application.

***Table 2.3**. Best MSE of the test set using several input parameter combinations.*

Combination	Algorithm			
	PSO	GWO	WOA	SMO
(T, U, P, WBT)	2.24E-02	2.75E-02	2.44E-02	2.56E-02
(T, DPT, G, P)	2.29E-02	3.36E-02	3.27E-02	2.60E-02
(DPT, U, P, WBT)	2.21E-02	2.34E-02	3.90E-02	2.54E-02
(DPT, G, P, WBT)	2.27E-02	2.74E-02	3.88E-02	2.62E-02
(T, U, P)	2.28E-02	2.34E-02	2.52E-02	2.44E-02

To further explore the individual impact of the four key environmental parameters identified by the Sobol index (precipitation, dew point temperature, temperature, and wind speed) on the predicted ILR, a case study analyzed how increasing each parameter by 10%, 20%, and 30% in a specific test case ($T = -1.4$°C, $DPT = -4.12$°C, $P = 0.08\ in/h$ and $U = 5.58\ kts$) affects the predicted ILR. As expected and consistent with the global sensitivity analysis (Section 4.2), precipitation exhibited the strongest influence, followed by dew point temperature, temperature, and wind speed (results in Table 2.4). For example, a 30% increase in precipitation led to a 14.58% decrease in predicted ILR, while the same increase for wind speed only resulted in a 4.37% increase in predicted ILR. This suggests that higher precipitation rates lead to lower ILRs, likely due to increased runoff as the liquid doesn't freeze before more liquid is added to the ice surface (Sanders & Barjenbruch, 2016).

***Table 2.4.** Impact of individual parameter variations on predicted ILR*

% parameter increase	P		DPT		T		U	
	ILR	% ILR change	ILR	% ILR change	ILR	% ILR change	ILR	% ILR change
10%	0.569	-4.86	0.618	3.26	0.588	-1.66	0.607	1.46
20%	0.540	-9.72	0.637	6.52	0.579	-3.33	0.616	2.91
30%	0.511	-14.58	0.657	9.79	0.569	-4.99	0.625	4.37

It's worth noting that the dataset used for training the model was drawn from a broad, geographically diverse range across the United States. This suggests that investigating the effects of site-specific factors could be valuable, potentially enhancing the model's predictive capabilities. Including such factors as additional inputs in the model might lead to further improvements in simulation accuracy. In addition, the ASOS data, including ice data and other meteorological variables, is collected at 1.5 metres above ground level. Therefore, environmental data used with this model should ideally be given at the same height (1.5 m) for optimal accuracy. Wind speed is particularly sensitive to the sensor height and requires conversion if measured at different heights (e.g., the standard 10-meter level). Established methods like log or power law profiles, or other calibrated approaches, can be used for wind speed conversion. However, the model's intended use with operational forecast models, which typically predict ASOS-measured environmental variables (e.g., precipitation, wind speed, temperature, dewpoint), allows for flexibility in data height. If 10-meter data is available, the model can be retrained on that configuration, and users should then provide inputs at the standard 10-meter height. Future research exploring vertical wind profiles and scaling methods holds promise for further refinement. In addition, while the current approach identifies suitable hyperparameters (e.g., number of nodes in the hidden layer), a more systematic exploration could potentially lead to further improvements. Employing Bayesian optimization to explore the hyperparameter space offers a promising avenue for identifying configurations that optimize both model performance and training efficiency. Moreover, incorporating techniques like knowledge-enhanced neural networks ((Karniadakis et al., 2021) ; (Snaiki & Wu, 2019), (Snaiki & Wu, 2022); (Naeini & Snaiki, 2024)) presents a promising avenue to potentially improve model performance. These networks leverage both data and underlying physical principles, offering the potential for more accurate and interpretable ILR predictions.

2.5 Concluding Remarks

In this study, the ILR was predicted using a feedforward neural network (FFNN) trained with various metaheuristic optimizers to overcome the limitations of gradient-based algorithms. The environmental data for freezing rain events were sourced from the Automated Surface Observing System (ASOS), with analysis focusing on six key parameters. A Sobol index-based global sensitivity analysis, utilizing polynomial chaos expansion coefficients, was conducted to assess the significance of these input parameters. The results revealed that only four input parameters - precipitation, temperature, dew point temperature, and wind speed - substantially influenced the response variance. Five optimization algorithms were evaluated for training the FFNN model: particle swarm optimization (PSO), grey wolf optimizer (GWO), whale optimizer (WOA), slime mold optimizer (SMO), and the standard stochastic gradient descent (SGD). The metaheuristic optimizers consistently outperformed SGD. Training set MSE values for PSO, GWO, WOA, SMO, and SGD were 2.19E-02, 2.24E-02, 2.21E-02, 2.42E-02, and 4.30E-02, respectively. This trend continued for testing performance, with PSO, GWO, and WOA achieving comparable MSE values (around 2.29E-02) and high correlation coefficients (above 0.80). This superior performance is attributed to the metaheuristic optimizers' high exploratory and exploitative behaviors, which enable them to avoid local optima effectively and converge rapidly toward the global optimum. Overall, the proposed model has the potential to enhance the meteorological community's ability to predict freezing rain accumulation.

2.6 References

Chaîné, P., & Castonguay, G. (1974). New approach to radial ice thickness concept applied to bundle-like conductors. *industrial meteorology—Study IV.Toronto: Environment Canada.*

Chang, S., McDaniels, T., Mikawoz, J., & Peterson, K. (2007). Infrastructure failure interdependencies in extreme events: power outage consequences in the 1998 Ice Storm. *Natural Hazards, 41*, 337–358.

Chen, Y., Li, P., Ren, W., Shen, X., & Cao, M. (2020). Field data–driven online prediction model for icing load on power transmission lines. *Measurement and Control, 53(1-2)*, 126–140. https://doi.org/https://doi.org/10.1177/0020294019878

DeGaetano, A., Belcher, B., & Spier, P. (2008). Short-Term Ice Accretion Forecasts for Electric Utilities Using the Weather Research and Forecasting Model and a Modified Precipitation-Type Algorithm. *Weather and Forecasting, 23*, 838–853. https://doi.org/https://doi.org/10.1175/2008WAF2006106.1

Fikke, S., Kristjánsson, J., & Kringlebotn Nygaard, B. (2008). *Modern Meteorology and Atmospheric Icing.* Atmospheric icing of power networks,Springer.

He, L., Luo, J., & Zhou, X. (2021). A Novel Deep Learning Model for Transmission Line Icing Thickness Prediction. (IEEE, Ed.) 733–738.

Jarrett, P., Yau, K.-H., & Morris, R. (2019). Update of the Reference Ice Thickness Amounts due to Freezing Rain for Canadian Codes and Standards . *Proceedings – Int. Workshop on Atmospheric Icing of Structures* , 23 – 28 .

Lenhard Jr., R. (1955). An Indirect Method for Estimating the Weight of Glaze on Wires. *American Meteorological Society, 36*, 1–5. https://doi.org/https://doi.org/10.1175/1520-0477-36.1.1

Mladenovic, N., & Hansen, P. (1997). Variable neighborhood search. *Computers & Operations Research, 24*, 1097-1100.

Niu, D., Wang, H., Chen, H., & Liang, Y. (2017). The General Regression Neural Network Based on the Fruit Fly Optimization Algorithm and the Data Inconsistency Rate for Transmission Line Icing Prediction. *Energies, 10(12)*(2066), 1-20.

Ruszczak, B., & Tomaszewski, M. (2014). Extreme Value Analysis of Wet Snow Loads on Power Lines. *IEEE Transactions on Power Systems, 30*, 457 - 462.

Ryerson, C., & Ramsay, A. (2007). Quantitative Ice Accretion Information from the Automated Surface Observing System. *ournal of Applied Meteorology and Climatology, 46*, 1423–1437.

Sheng, C., Tang, Q., & Hong, H. (2023). Estimating and Mapping Extreme Ice Accretion Hazard and Load Due to Freezing Rain at Canadian Sites. *International Journal of Disaster Risk Science*, 127–142.

Snaiki, R., & Wu, T. (2022). Knowledge-Enhanced Deep Learning for Simulation of Extratropical Cyclone Wind Risk. *Atmosphere, 13(5)*(757), 14. https://doi.org/https://doi.org/10.3390/atmos13050757

Tomaszewski, M., Ruszczak, B., Michalski, P., & Zator, S. (2019). The study of weather conditions favourable to the accretion of icing that pose a threat to transmission power lines. *International Journal of Critical Infrastructure Protection, 25*, 139-151.

Armenakis, C., & Nirupama, N. (2014). Urban impacts of ice storms: Toronto December 2013. *Natural Hazards, 74*, 1291–1298.

Chang, S., McDaniels, T., Mikawo, J., & Peterson, K. (2012). Infrastructure Failure Interdependencies in Extreme Events: The 1998 Ice Storm. *Disaster Risk and Vulnerability: Mitigation through Mobilizing Communities and Partnerships, 275*.

Chen, S., Dai, D., Huang, X., & Sun, M. (2012). Short-Term Prediction for Transmission Lines Icing Based on BP Neural Network. (IEEE, Ed.)

Dai, D., Huang, X.-T., Dai, Z., Hao, Y., Li, L., & Fu , C. (2013). Regression model for transmission lines icing based on support vector machine. *High Voltage Eng, 39*, 2822–2828.

Du, X., Zheng, Z., Tan, S., & Wang, J. (2010). The study on the prediction method of ice thickness of transmission line based on the combination of GA and BP neural network. (IEEE, Ed.) 1-4.

Geem, Z., KIM, J., & Loganathan, G. (2001). A New Heuristic Optimization Algorithm: Harmony Search. *simulation, 76*.

Goodwin, T., Mozer, J., & DiGioia, A. (1983). Predicting ice and snow loads for transmission line design. *Predict. Ice Snow Loads Trans. Line Design*, 267–273.

Huang, X., & Li, J. (2012). Icing thickness prediction model using BP Neural Network. (IEEE, Ed.)

Huang, X., Xu, J., Yang, C., Wang, J., & Xie , J. (2014). Transmission line icing prediction based on data driven algorithm and LS-SVM. *Autom. Electr. Power Sys, 38*, 81–86.

Imai, I. (1953). Studies of ice accretion. *Res. Snow Ice, 1*, 35-44.

Jeong, D., Cannon, A., & Zhang, X. (2019). Projected changes to extreme freezing precipitation and design ice loads over North America based on a large ensemble of Canadian regional climate model simulations. *Natural Hazards and Earth System Sciences, 19*, 857–872.

Jeong, D., Sushama, L., Vieira, M., & Koenig, K. (2018). Projected changes to extreme ice loads for overhead transmission lines across Canada. *Sustainable Cities and Society, 39*, 639-649.

Jones, K. (1998). A simple model for freezing rain ice loads. *Atmospheric Research, 46*, 87–97.

Karniadakis, G., u, L., Kevrekidis, Y., & Perdikaris, P. (2021). Physics-informed machine learning. *Nature Reviews Physics, 3*, 422–440.

Kennedy, J., & Eberhart, R. (1995). Particle swarm optimization. *IEEE*, 1942-1948.

Kirkpatrick, S., Gelatt Jr, C., & Vecchi, M. (1983). Optimization by simulated annealing. *science, 220*, 671-680.

Li, P., Li, Q., Cao, M., Gao, S., & Huang, H. (2011). Time series prediction for icing process of overhead power transmission line based on BP neural networks. (IEEE, Ed.) *Proceedings of the 30th Chinese Control Conference*, 5315-5318.

Lozowski, E., & Makkonen, L. (2005). Fifty years of progress in modelling the accumulation of atmospheric ice on power network equipment.

Ma, T., & Niu , D. (2016). Icing Forecasting of High Voltage Transmission Line Using Weighted Least Square Support Vector Machine with Fireworks Algorithm for Feature Selection. *Applied Sciences, 6*(438).

Ma, T., Niu , D., & Fu, M. (2016). Icing Forecasting for Power Transmission Lines Based on a Wavelet Support Vector Machine Optimized by a Quantum Fireworks Algorithm. *Applied Sciences, 6*(54).

Makkonen, L. (1984). Modeling of Ice Accretion on Wires. *Journal of Applied Meteorology and Climatology, 23*(6), 929–939.

Makkonen, L. (1998). Modeling power line icing in freezing precipitation. *Atmospheric Research, 46*(1–2), 131-142.

Mallat, S., & Zhang, Z. (1993). Matching pursuits with time-frequency dictionaries. (IEEE, Ed.) *Transactions on signal processing, 41*, 3397-3415.

Naeini, S., & Snaiki, R. (2024). A physics-informed machine learning model for time-dependent wave runup prediction. *Ocean Engineering, 295*(116986).

Ojha, V., Abraham, A., & Snášel, V. (2017). Metaheuristic design of feedforward neural networks: A review of two decades of research. *Engineering Applications of Artificial Intelligence, 60*, 97-116.

Pati, Y., Rezaiifar, R., & Krishnaprasad, P. (1993). Orthogonal matching pursuit: recursive function approximation with applications to wavelet decomposition. *IEEE*, 40-44.

Rashedi, E., Nezamabadi-pour, H., & saryazdi, s. (2009). GSA: a gravitational search algorithm. *Information sciences, 179*, 2232–2248.

Sanders, K., & Barjenbruch, B. (2016). Analysis of Ice-to-Liquid Ratios during Freezing Rain and the Development of an Ice Accumulation Model. *Weather and Forecasting, 31*(4), 1041–1060.

Shabani, M., Jamali, A., Snaiki, R., & Rahem, A. (2022). Prediction of Ice Accretion on Transmission Lines using Hybrid Particle Swarm Optimization-based Artificial Neural Networks.

Snaiki, R. (2024). Performance-based ice engineering: a data-driven multi-scale approach. *arXiv preprint arXiv:2401.13860*, 24.

Snaiki, R., & Wu, T. (2019). Knowledge-enhanced deep learning for simulation of tropical cyclone boundary-layer winds. *Journal of Wind Engineering and Industrial Aerodynamics, 194*(103983).

Stieltjes, T. (1884). Quelques recherches sur la théorie des quadratures dites mécaniques. 409-426.

Sun, W., & Wang, C. (2019). Staged icing forecasting of power transmission lines based on icing cycle and improved extreme learning machine. *Journal of Cleaner Production, 208*, 1384-1392.

Wu , T., & Snaiki, R. (2022). Applications of Machine Learning to Wind Engineering. *Frontiers in Built Environment, 8*(811460).

Xu, X., Niu, D., Wang, P., Lu, Y., & Xia, H. (2015). The Weighted Support Vector Machine Based on Hybrid Swarm Intelligence Optimization for Icing Prediction of Transmission Line. *Mathematical Problems in Engineering*.

Yin, S., Lu, Y., Wang, Z., Li, P., & Xu, K. (2012). Icing thickness forecasting of overhead transmission line under rough weather based on CACA-WNN. *Electr. Power Sci. Eng,, 11*.

Ying, Z.-R., & Su, X.-L. (2014). Icing thickness forecasting of transmission line based on particle swarm algorithm to optimize SVM. *J. Electr. Power, 29*, 6-9.

Zarnani, A., Musilek, P., Shi, X., Ke, X., He, H., & Greiner, R. (2012). Learning to predict ice accretion on electric power lines. *Engineering Applications of Artificial Intelligence, 25*(3), 609-617.

Zhang, Z., Huang, H., Jiang, X., Hu, J., & Sun, C. (2012). Analysis of ice growth on different. *Diangong Jishu Xuebao (Transact. China Electrotech. Soc.), 27*, 35–43.

CHAPITRE 3

ARTICLE 2: TOWARDS ACCURATE ICE ACCRETION AND GALLOPING RISK MAPS FOR QUEBEC: A DATA-DRIVEN APPROACH

Abdeslam Jamali [1], Reda Snaiki [2,*], Ahmed Rahem [1]

[1] *Department of Applied Sciences, Université du Québec à Chicoutimi, Chicoutimi, QC, Canada*

[2] *Department of Construction Engineering, École de Technologie Supérieure, Université du Québec, Montréal, Canada*

[*] *Corresponding author. Email:* reda.snaiki@etsmtl.ca

Submitted on November 5, 2024, to *Cold Regions Science and Technology*.

Received in revised form 3 February 2025; Accepted 16 February 2025

Available online 17 February 2025

Acknowledgements

This work was partly supported by the Natural Sciences and Engineering Research Council of Canada (NSERC) [grant number CRSNG RGPIN 2022-03492].

Résumé

L'accumulation de glace représente une menace importante pour les infrastructures et la sécurité publique, en particulier dans les régions sujettes à des conditions hivernales rigoureuses. Une cartographie précise des risques d'accumulation de glace est essentielle pour une gestion et une atténuation efficaces des risques. Bien que des progrès significatifs aient été réalisés dans la cartographie de ces risques, la plupart des cartes existantes reposent sur des valeurs calculées plutôt que sur des mesures directes, ce qui peut entraîner des imprécisions. Pour pallier ces limites, cette étude utilise les données de mesures de terrain du réseau de glacimètres d'Hydro-Québec pour développer des cartes affinées de l'accumulation de glace au Québec. Les épaisseurs maximales annuelles d'accumulation de glace sont extraites, et une analyse rigoureuse d'ajustement de distributions probabilistes est appliquée pour générer des valeurs correspondant à des périodes de retour de 10, 30 et 50 ans. Ces valeurs sont interpolées en utilisant les techniques d'interpolation pondérée à distance inverse (IDWI) et de krigeage, permettant une évaluation comparative des méthodes d'interpolation. De plus, les risques de galop sont évalués à l'aide du cadre d'ingénierie de la glace basée sur la performance (PBIE), produisant des cartes de risque de galop pour différentes périodes de retour. En intégrant des données empiriques et en comparant les approches d'interpolation, cette recherche améliore la précision des cartes de l'accumulation de glace et des risques de

galop, offrant des évaluations des dangers plus fiables pour les infrastructures du Québec.

Mots-clés : Accumulation de glace ; Risque de galop ; Cartographie des dangers ; Périodes de retour ; Valeurs extrêmes.

Abstract

Ice accretion poses a significant threat to infrastructure and public safety, particularly in regions prone to severe winter weather. Accurate ice accretion hazard mapping is essential for effective risk management and mitigation. While substantial progress has been made in mapping these hazards, most existing ice accretion maps rely on calculated ice accretion values rather than direct measurements, leading to potential inaccuracies. To address these limitations, this study leverages field measurement data from Hydro-Québec's glacimètre network to develop refined ice accretion maps for Quebec. The maximum annual ice accretion thicknesses are extracted, and a rigorous probability distribution fitting analysis is applied to generate 10-, 30-, and 50-year return period values. These values are interpolated using both inverse-distance weighted interpolation (IDWI) and kriging techniques, allowing for a comparative evaluation of interpolation methods. Additionally, galloping risks are assessed using the Performance-Based Ice Engineering (PBIE) framework, producing galloping risk maps for various return periods. By incorporating real-world data and comparing interpolation approaches, this research enhances the accuracy of ice accretion and galloping risk maps, providing more reliable hazard assessments for Quebec's infrastructure.

Keywords: Ice accretion; galloping risk; hazard mapping; Return periods; Extreme values.

3.1 Introduction

Ice accretion on infrastructure, such as power transmission lines, poses a significant hazard in cold climates. Accumulations of ice during freezing rain, wet snow events, and other atmospheric conditions can lead to severe structural failures, power outages, and risks to public safety. This phenomenon is particularly concerning in regions like Quebec, where harsh winter conditions often result in extensive ice buildup. One of the most notable examples is the North American Ice Storm of January 1998, which impacted Canada and the United States. The storm's destructive force led to an estimated $4 billion USD in damages, with over 4 million residents losing power (Mittermeier et al., 2022). Therefore, understanding and predicting ice accretion effects are critical for mitigating risks and ensuring the reliability of essential infrastructure.

Due to the challenges of direct measurement, ice accretion is often estimated using various modelling techniques. Obtaining accurate, widespread data on ice accretion is difficult, as measurement stations are sparse, and ice accretion events are highly localized and dependent on microclimatic conditions. Various models have been proposed to estimate ice accretion, ranging from physics-based to data-driven approaches (Snaiki et al., 2024). Traditional physics-based models of ice accretion rely on simplified mathematical formulations and fundamental physical laws (Goodwin et al., 1983; Makkonen, 1998; Zhang et al., 2012). While these models provide a valuable theoretical framework, they may fall short in capturing the complexities of ice accretion in real-world conditions (He et al., 2021). Data-driven models, on the other hand, leverage diverse data sources, such as the output of numerical models, to establish relationships between input variables (e.g., meteorological conditions, conductor geometry) and ice accretion. These models can be constructed using various machine learning techniques, ranging from simple statistical methods (Chaîné and Castonguay, 1974; Jones, 1998) to complex deep neural networks (Snaiki et al., 2024). While simplified autoregressive formulas offer computational efficiency and ease of implementation, their reliance on predefined basis functions and autoregressive structures may limit their ability to accurately model complex dynamic systems like ice accretion (Jeong et al., 2019; Sheng et al., 2023). Machine learning approaches, such as deep neural networks, provide a promising alternative for rapidly predicting ice accretion. These models can effectively capture nonlinear dynamics without relying on simplified assumptions or linearization, making them well suited for the complex nature of ice accretion (Niu et al., 2017; Ma et al., 2016; Sun and Wang, 2019). While machine learning approaches offer several advantages, they also have certain limitations. One significant drawback is the reliance on large amounts of high-quality data. Insufficient or biased data can lead to inaccurate predictions and limit the generalizability of the models. Additionally, machine learning models can be computationally expensive to train and deploy, especially for complex models with many parameters. Furthermore, interpreting the internal workings of machine learning models can be challenging, making it difficult to understand the underlying physical processes driving ice accretion. This can hinder the development of physically interpretable models that can be used to gain insights into the underlying mechanisms.

Ice accretion hazard maps for Canada have been developed to assess the severity and spatial distribution of ice loads due to freezing rain events. These maps are typically based on probabilistic modelling techniques, such as the Gumbel distribution, to estimate extreme ice accretion events over various return periods. These maps have played a crucial role in establishing design standards for Canadian infrastructure. For instance, Yip (1995) generated

30-year return period ice accretion values for a 25 mm diameter rod at various locations across Canada, using the Chaîné and Castonguay (1974) model. Jarrett et al. (2019) also generated 50-year return period ice accretion hazard maps using a 25 mm diameter rod, employing the Gumbel distribution to fit maximum annual ice accretion thickness. Recent advancements in ice accretion hazard mapping have involved the use of multiple ice accretion models and statistical techniques. Sheng et al. (2023) refined and expanded existing hazard maps by applying different models and distributions to various Canadian regions. The Gumbel distribution was found to be suitable for regions prone to ice accretion, while the lognormal distribution was more appropriate for areas with moderate or negligible ice accretion. While significant progress has been made in ice accretion hazard mapping, it's important to note that most existing maps rely on calculated ice accretion values rather than direct measurements. This is due to the inherent challenges of accurately measuring ice accumulation on structural surfaces. The choice of ice accretion model can significantly influence the resulting hazard maps (Sheng et al., 2023), making it difficult to determine the optimal model for all regions.

To overcome the limitations of existing ice accretion models in generating accurate hazard maps, this study leverages field measurement data from Hydro-Québec's extensive glacimètre network to develop refined ice accretion maps for the province of Quebec. By incorporating real-world data, this research aims to improve the predictive capabilities of current models and provide more reliable assessments of ice storm risks. Maximum annual ice accretion thicknesses were extracted from the glacimètre data for each station and subjected to a comprehensive probability distribution fitting analysis. The resulting 10-, 30-, and 50-year return period values were then interpolated onto a high-resolution map using both inverse-distance weighted interpolation (IDWI) and ordinary kriging techniques. This comparative analysis evaluates the impact of interpolation methods on the accuracy and reliability of the generated ice accretion hazard maps. To further assess the potential risks associated with ice accretion, this study extends the analysis to include galloping risk assessment. The Performance-Based Ice Engineering (PBIE) framework is employed to generate galloping risk maps corresponding to various return periods. The galloping risk is assessed numerically using the double galloping amplitude. The influence of interpolation techniques on the accuracy of these galloping risk maps is also examined.

3.2 Meteorological Data and Statistics of Ice Accretion

3.2.1 Historical data

This study leverages a comprehensive dataset of ice accretion and wind speed data collected from Hydro-Québec's extensive glacimètre network, established in 1974 (Laflamme, 2004). Strategically located across Quebec, with a particular emphasis on the St. Lawrence Valley, these stations provide detailed measurements of ice accretion on cylindrical surfaces oriented towards each cardinal direction. The glacimètre design allows for precise characterization of icing events, including type, orientation-specific accumulation, thickness, and duration. This rich dataset has served as a cornerstone for developing robust design criteria for overhead transmission line systems in the region, solidifying Hydro-Québec's network as a leading resource for ice accretion research in North America. The present analysis focuses on the period between 1975 and 2020, examining mean wind speed and equivalent ice accretion data from 55 stations distributed across Quebec as depicted by Figure 3.1. For each station, maximum annual ice accretion thicknesses were extracted and subjected to a rigorous probability distribution fitting analysis. It is important to note that the glacimètre measures the equivalent radial thickness of ice on a 30 mm conductor, assuming a flat terrain (Périard, 2018).

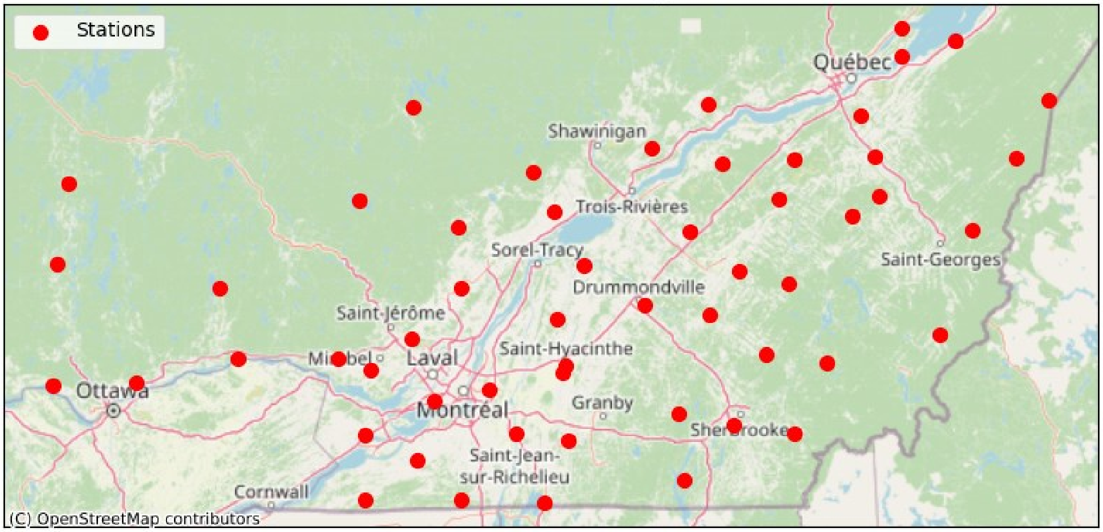

Figure 3.1 *Glacimetre Station Network in Quebec*

3.2.2 Probabilistic analysis of ice accretion thickness

To model the extreme ice accretion events, three common probability distributions were considered as proposed by Sheng et al. (2023): the Gumbel, Generalized Extreme Value (GEV), and lognormal distributions. Given the sensitivity of the Generalized Pareto Distribution (GDP) to threshold selection, the peak-over-threshold approach was not employed in this study (Sheng et al. 2023). Figure 3.2 illustrates the goodness of fit for these distributions at six representative stations: Iberville, Montréal-A, Québec-A, Saint-Hubert-A, Honfleur and Montmagny. The results clearly demonstrate significant regional variability in ice accretion, with stations like Honfleur experiencing substantially more severe events compared to those at Montmagny. While both the Gumbel and GEV distributions provided adequate fits for most stations, the lognormal distribution proved less suitable, particularly for sites like Iberville, Québec-A, and Montmagny. Although the optimal distribution choice was found to be site-specific, the Gumbel distribution was ultimately selected for its overall performance and compatibility with the observed data.

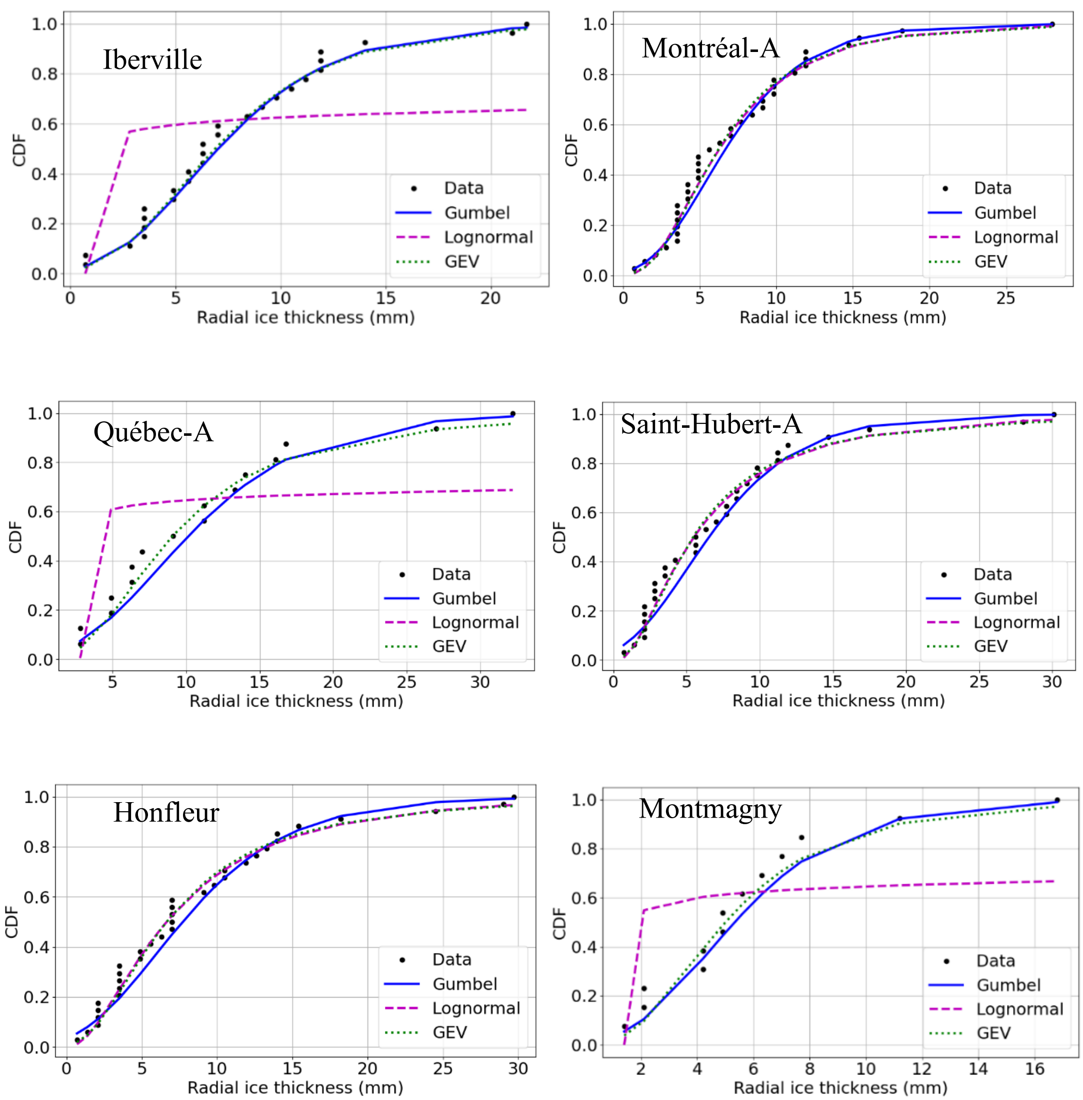

Figure 3.2 *Probability distribution fitting for a maximum annual ice accretion thickness*

3.3 Ice Accretion Hazard Maps

Given the superior performance of the Gumbel distribution as demonstrated in Section 3.2, it was selected for the development of ice accretion hazard maps. To determine the T-year return period value of the annual maximum ice accretion thickness (I_T), the following equation was employed (Sheng et al., 2023):

$$1 - \frac{1}{T} = p_0 + (1 - p_0)F_I(I_T) \tag{1}$$

where p_0 represents the probability of zero ice accretion, and $F_I(I_T)$ denotes the fitted Gumbel distribution. The calculated T-year return period values were then interpolated onto a high-resolution map using both inverse-distance weighted interpolation (IDWI) and ordinary kriging techniques. Specifically, the maximum annual ice accretion thicknesses for 10, 30, and 50-year return periods were estimated and visualized using these interpolation methods in Figure 3.3.

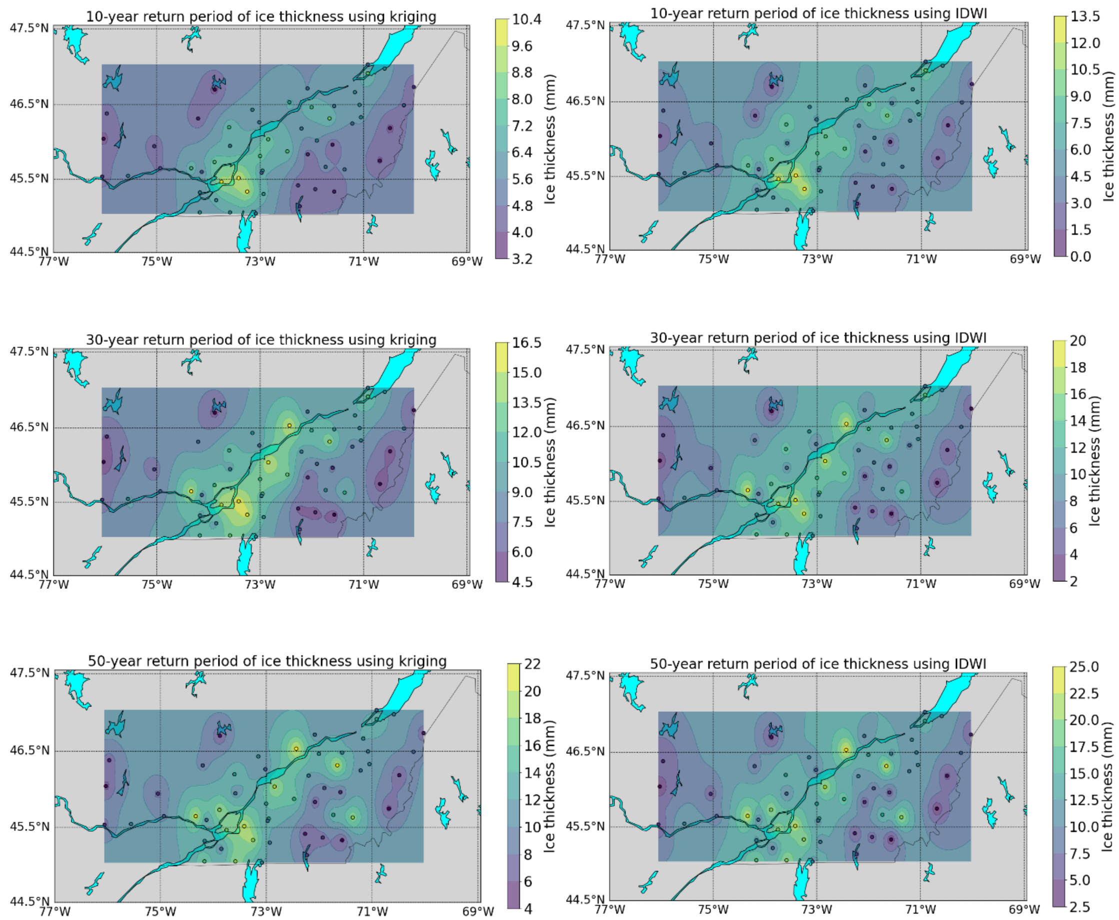

***Figure 3.3** Estimated ice accretion hazard maps for Quebec (10, 30, and 50-year return periods)*

The generated ice accretion hazard maps clearly depict significant spatial variability across the region. A pronounced trend of increased ice thickness near the St. Lawrence River is evident, suggesting that these areas are more susceptible to severe icing events compared to other regions. This observation underscores the influence of geographical and climatic factors, such as proximity to water bodies, prevailing winds, and terrain elevation, on ice accretion patterns. As expected, the ice thickness increases with increasing return periods, maintaining a generally consistent spatial pattern but with varying magnitudes. For example, the 50-year return period map exhibits a maximum ice accretion of 22 mm, while the 10-year return period map shows a maximum of 10 mm using the kriging approach. Interestingly, the kriging technique produces smoother maps compared to the IDWI technique. However, IDWI tends to yield slightly higher ice accretion values. For instance, at the 50-year return period, IDWI estimates a maximum of 25 mm compared to 22 mm from kriging. Similar differences are observed for the 30- and 10-year return periods. Despite these minor discrepancies, the overall spatial distribution of ice accretion remains consistent across all three return periods, reflecting the underlying geographical and climatic influences. The choice of interpolation technique may introduce some variability in the specific values, but the general patterns and trends remain reliable for assessing ice accretion risk in the region.

3.4 Galloping Risk Maps for Quebec

To assess the risk of galloping-induced vibrations on iced conductors, this section leverages the ice accretion hazard maps developed in Sect. 3.3. The Performance-Based Ice Engineering (PBIE) framework, a recently developed approach for evaluating ice storm risks, is employed to generate galloping risk maps corresponding to various return periods (Snaiki, 2024). The PBIE framework, designed for both local and regional applications, utilizes advanced data-driven techniques, such as machine learning, to efficiently predict risks like galloping. By sequentially assessing hazards, structural interactions, and potential damage, the PBIE enables real-time risk estimation across extensive areas. Its versatility extends to various structures, from transmission lines to wind turbines, supporting both emergency response and long-term planning in the face of climate change. The galloping amplitude of transmission lines subjected to wind and ice is estimated using a simplified semi-empirical approach (Lu and Chan, 2009; Lu and Chakrabarti, 2023). While more sophisticated theories can be integrated into the PBIE framework, this simplified model provides a practical means of assessing galloping-induced risk. The galloping risk will be quantified in terms of the double galloping amplitude. A concise overview of galloping instability, conditions, and the employed dynamic model will be presented in the subsequent sections.

3.4.1 Galloping Instability and Conditions

Galloping is a type of wind-induced instability that can result in significant, low-frequency oscillations in transmission lines, particularly when ice accretion is present. To predict the onset of galloping, two primary criteria must be satisfied (den Hartog, 1932). The first criterion involves the Den Hartog coefficient, a_g, which must be negative:

$$a_g = C_d + \frac{dC_l}{d\alpha} < 0 \tag{2}$$

where C_d represents the drag coefficient, C_l denotes the lift coefficient, and α is the angle of attack. The second criterion for galloping instability pertains to the total system damping, ξ, which must satisfy the following inequality:

$$\xi = \xi_s + \xi_a < 0 \tag{3}$$

where ξ_s represents structural damping and ξ_a denotes aerodynamic damping. To fulfill the second criterion for galloping instability, the wind speed must exceed a critical wind speed value, denoted as V_c, which can be calculated using the following expression:

$$V_c = -\frac{4.\omega_n.\xi_s.m_s}{\rho_0.d_c.a_g} \tag{4}$$

where ω_n represents the natural angular frequency, m_s is the mass of the conductor, ρ_0 denotes the density of ice and d_c is the conductor's diameter.

3.4.2 Dynamic model of the transmission line system

A semi-empirical modelling approach is used in this study to simulate the galloping amplitude of transmission lines under various wind and ice loading conditions. This methodology, which integrates finite element analysis and a 3-degree-of-freedom system, provides a computationally efficient and accurate means of assessing galloping behaviour. The model has been rigorously validated against comprehensive parametric studies and field measurements from North American transmission systems. The resulting semi-empirical equation, presented below, enables the estimation of galloping amplitudes for both single and bundled conductors, regardless of support type (suspension or dead-end). The vertical galloping amplitude, denoted as A_G, is calculated as follows:

$$A_G = {}^{G}\!/_{f} \tag{5}$$

The galloping factor, G, characterizing the severity of galloping, is typically assigned a value of 0.75 m/s for North American transmission lines based on extensive field observations. The natural frequency of the conductor in the vertical direction, denoted as f, is a critical factor in determining galloping susceptibility. For sagged conductor spans with fixed-end conditions, f can be calculated using the following equation:

$$f = \frac{k}{L}\sqrt{\frac{H}{m}} \tag{6}$$

The natural frequency f is influenced by several factors, including the conductor span length L, static tension H, mass per unit length m, and a parameter k related to the number of galloping loops. For a one-loop galloping mode, k can be determined as a function of the conductor tension (T) by the following equation:

$$\tan(k\pi) = k\pi - \frac{4(k\pi)^3}{K_c \frac{L^3}{T^3} m^2 g^2} \quad (7)$$

The conductor stiffness, K_c, is calculated as the product of the equivalent elastic modulus E and the cross-sectional area A, divided by the span length L. The single galloping amplitude serves as a basis for determining the double galloping amplitude Y, which can be expressed as $Y = 2A_G$.

3.4.3 Galloping risk maps

The PBIE framework was utilized to evaluate the risk of vertical galloping on iced conductors, considering ice accretion scenarios corresponding to return periods of 10, 30, and 50 years, as delineated in Sect.3.3. To assess the influence of interpolation technique, design maps were generated using both ordinary kriging and inverse-distance weighted interpolation (IDWI). Limit states (LS) were established based on the double galloping amplitude, Y, and defined as the difference between engineering demand and structural capacity for each damage state. A limit state of $LS \geq 0$ indicates failure. Three risk categories were defined according to the magnitude of Y: low-risk ($Y \leq 2\ m$), moderate risk ($2 < Y \leq 3\ m$), and high-risk ($Y > 3\ m$).

It is well documented that ice accretion on fixed conductors often exhibits a crescent-shaped profile. Consequently, accurate modelling of this profile is crucial for realistic representation of wind-induced aerodynamic loads. Consistent with previous research (Rossi et al., 2020; Davalos et al., 2023; Snaiki, 2024), a semi-elliptical shape was adopted to model the ice accretion. The drag coefficient was determined based on experimental wind tunnel data from Rossi et al. (2020). Other relevant structural parameters included: $L = 172.4m$,

$E = 70GPa$, $sag = 3.39m$, $m = 1.3kg/m$, and $A = 4.35 * 10^{-4}m^2$. To incorporate uncertainties in the structural parameters within the PBIE framework, a limited number of parameters were treated as random variables. Specifically, the conductor diameter was assumed to follow a normal distribution with a mean of 23.55 mm and a coefficient of variation of 0.05. The modulus of elasticity was modelled as a log-normal distribution with a mean of 70 GPa and a coefficient of variation of 0.03. Wind hazard maps, corresponding to the same return periods as the ice accretion maps, were developed using a comparable methodology to assess the potential for galloping. Figure 3.4 illustrates the galloping risk maps for return periods of 10, 30, and 50 years, generated using ordinary kriging interpolation.

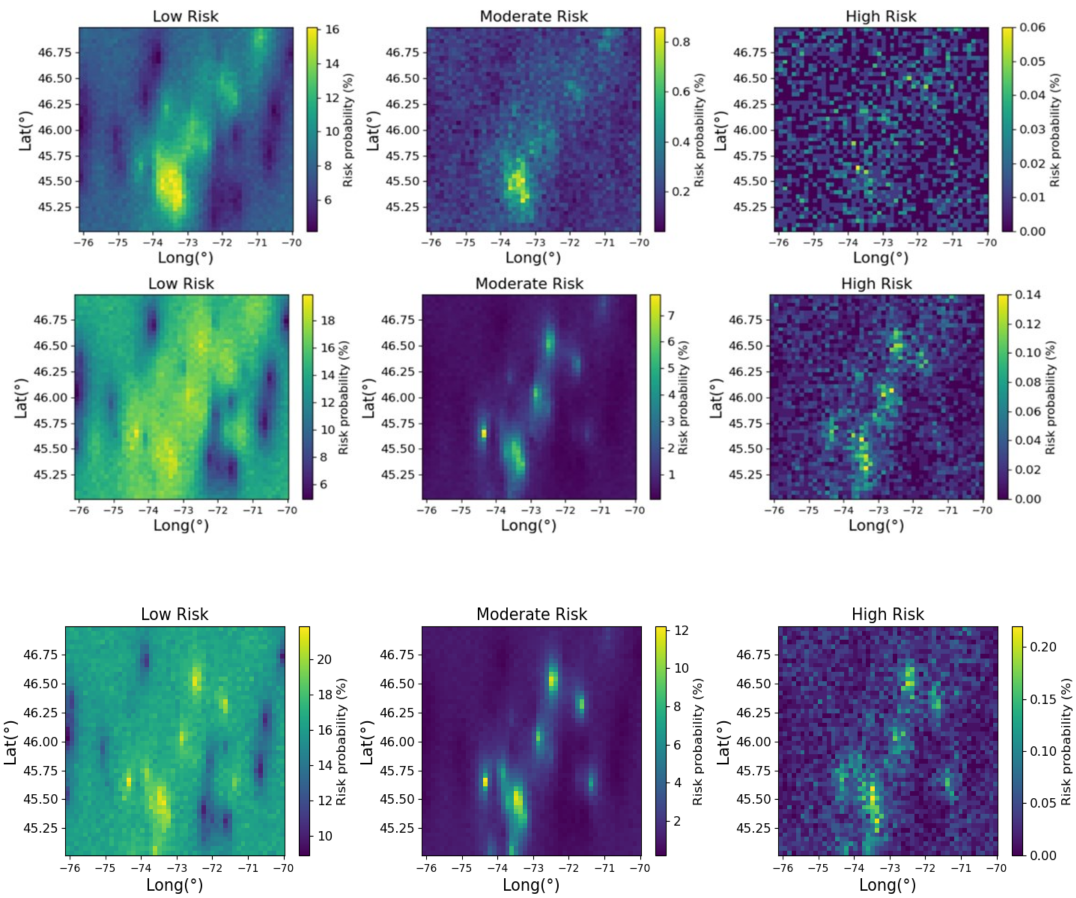

Figure 3.4 *Galloping-induced risk maps estimated for 10 years (top), 30 years (middle), and 50 years (bottom) return periods using kriging interpolation.*

The galloping risk maps, corresponding to return periods of 10, 30, and 50 years, provide valuable insights into the spatial distribution and severity of galloping risk within the region. Analysis of these maps enables the identification of critical areas, facilitating the assessment of potential infrastructure impacts and informed decision-making for risk mitigation. While the overall spatial distribution of risk remains relatively consistent across all return periods, specific regions, such as the St. Lawrence Valley, particularly in the southern portion, consistently exhibit higher-risk levels for all three risk categories. This is attributable to the same underlying factors influencing galloping susceptibility, including topography and meteorological conditions. Although the general risk pattern persists, notable variations in risk-level intensity are evident. For example, in the southern part of the St. Lawrence Valley (near the island of Montreal), the risk probability for the low-risk category increases from approximately 16% for a 10-year return period to nearly 22% for a 50-year return period. Similarly, the risk probability in the same region for the high-risk category increases from approximately 0.06% to 0.21% over the same return period. Similar maps were also generated using the IDWI technique, as depicted in Figure 3.5.

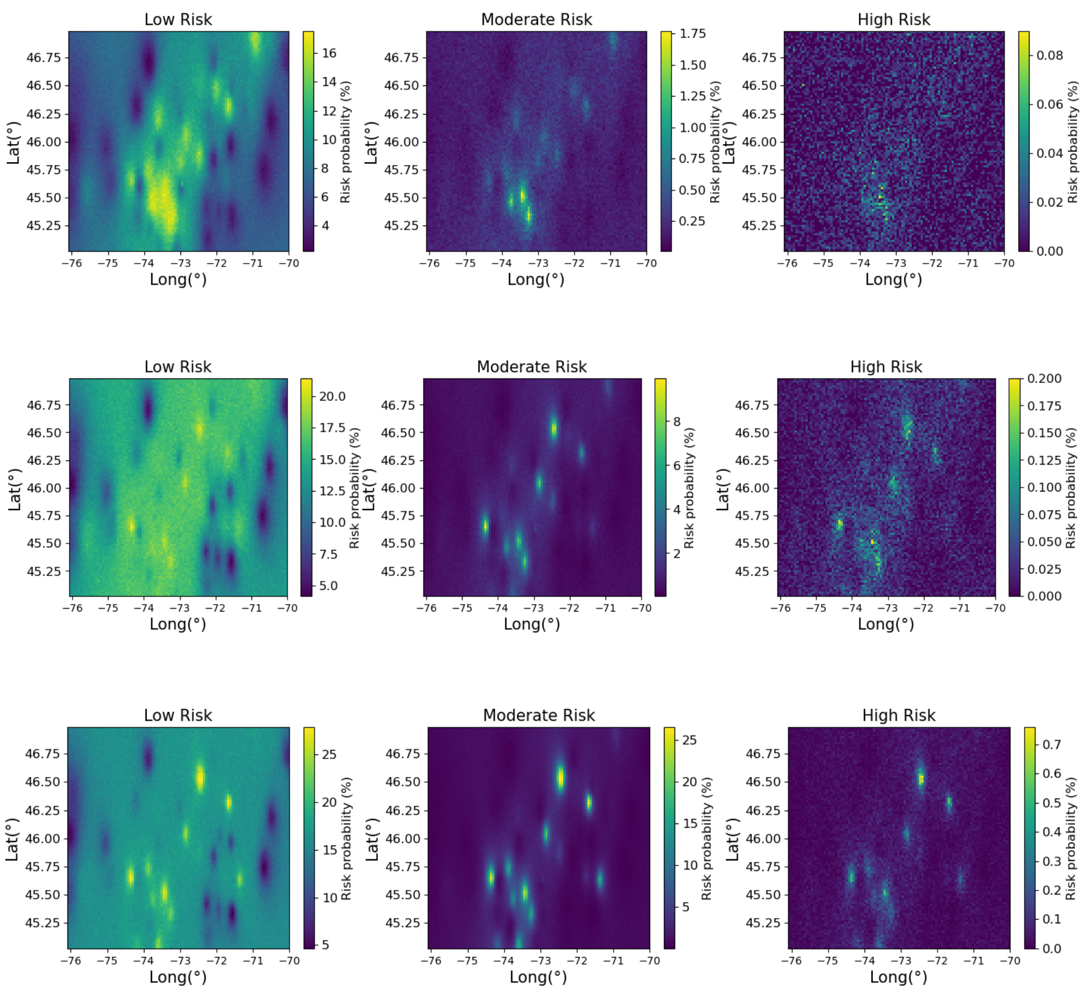

***Figure 3.5** Galloping-induced risk maps estimated for 10 years (top), 30 years (middle), and 50 years (bottom) return periods using the IDWI technique*

The overall spatial distribution of risk remains consistent between the IDWI and ordinary kriging maps. Despite overall similarities in the risk maps generated using different interpolation techniques, notable variations in risk intensity were observed. IDWI maps generally produced higher-risk values compared to ordinary kriging. For instance, the risk probability for the low-risk category increased from approximately 22% to 28% for a 50-year return period using IDWI. Similarly, the risk probability for the high-risk category rose from 0.21% to 0.74% for a 50-year return period. The choice of interpolation technique can influence the smoothness and detail of the generated maps. IDWI, being a distance-based method, may introduce more localized variations in risk, especially in areas with sparse data. Ordinary kriging, on the other hand, tends to produce smoother maps by considering the spatial correlation between data points.

To gain a deeper understanding of the factors influencing galloping risk, it's recommended to overlay geographic features (e.g., topography, vegetation, land use) on the risk maps. This can help identify correlations between environmental conditions and risk levels. The accuracy of the risk assessment depends on the quality of the input data, such as meteorological data, conductor characteristics, and ice accretion models. The galloping risk assessment model used might have limitations in capturing certain factors or scenarios. For instance, in this case study, a simplified semi-empirical modelling approach was used to simulate the galloping amplitude of transmission lines. In addition, a uniform grid network was used. However, a more accurate approach would integrate the exact layout of transmission lines within the PBIE framework. Climate change could also impact the frequency and severity of galloping events. Incorporating climate change projections into future risk assessments is essential. Overall, the generated maps can be used to prioritize areas for risk assessment, inspection, and maintenance. Regions with consistently high-risk levels (in yellow) should be prioritized for targeted inspections and mitigation measures, such as conductor modifications, improved ice management practices, or installation of galloping dampers. The maps provide valuable information for long-term planning, including infrastructure upgrades and risk-based decision-making.

3.5 Concluding Remarks

In this study, an enhanced methodology was proposed for generating ice accretion and galloping risk maps for Quebec by utilizing real-world field measurement data from Hydro-Québec's glacimètre network. By combining maximum annual ice accretion values with interpolation techniques, such as inverse distance weighting and kriging, accurate maps were developed for 10-, 30-, and 50-year return periods. Furthermore, by applying the Performance-Based Ice Engineering (PBIE) framework, the analysis was extended to include galloping risk, a critical factor for transmission line safety under severe icing conditions. The results indicate significant spatial variability in both ice accretion and galloping risk across the province, particularly in the St. Lawrence Valley region. This study highlights the importance of using field measurement data to improve the accuracy and reliability of hazard maps. It also underscores the influence of interpolation methods on risk predictions, emphasizing the need for careful selection of modelling techniques based on regional characteristics. Future work should focus on refining these methods and integrating climate change projections to ensure long-term resilience of critical infrastructure in ice-prone regions.

3.6 References

Chaîné, P.M. and Castonguay, G., 1974. New approach to radial ice thickness concept applied to bundle-like conductors (Vol. 4). Environment Canada, Atmospheric Environment.

Davalos, D., Chowdhury, J. and Hangan, H., 2023. Joint wind and ice hazard for transmission lines in mountainous terrain. Journal of Wind Engineering and Industrial Aerodynamics, 232, p.105276.

Den Hartog, J.P., 1932. Transmission line vibration due to sleet. Transactions of the American Institute of Electrical Engineers, 51(4), pp.1074-1076.

Goodwin, T., Mozer, J.D., DiGioia, A.M. and Power, B.A., 1983, June. Predicting ice and snow loads for transmission line design. In Proc. First Int. Workshop on Atmospheric Icing of Structures (pp. 267-273).

He, L., Luo, J. and Zhou, X., 2021, March. A novel deep learning model for transmission line icing thickness prediction. In 2021 IEEE 5th Advanced Information Technology, Electronic and Automation Control Conference (IAEAC) (Vol. 5, pp. 733-738). IEEE.

Jarrett, P., Yau, K.H. and Morris, R., 2019, June. Update of the reference ice thickness amounts due to freezing rain for Canadian codes and standards. In Proceedings of the International Workshop on Atmospheric Icing of Structures (pp. 23-28).

Jeong, D.I., Cannon, A.J. and Zhang, X., 2019. Projected changes to extreme freezing precipitation and design ice loads over North America based on a large ensemble of Canadian regional climate model simulations. Natural Hazards and Earth System Sciences, 19(4), pp.857-872.

Jones, K.F., 1998. A simple model for freezing rain ice loads. Atmospheric research, 46(1-2), pp.87-97.

Jones, K.F., Ramsay, A.C. and Lott, J.N., 2004. Icing severity in the December 2002 freezing-rain storm from ASOS data. Monthly weather review, 132(7), pp.1630-1644.

Laflamme, J., 2004. La mesure des dépôts de verglas. Rapport interne d'Hydro-Québec.

Lu, M.L. and Chan, J.K., 2009. A Rational Design Equation for Galloping Power Lines. In Int. Conference on Ultra-High Voltage Transmission, Beijing, China.

Lu, M.L. and Chakrabarti, D., 2023. Design ice and wind on overhead transmission lines in British Columbia. Cold Regions Science and Technology, 214, p.103960.

Ma, T., Niu, D. and Fu, M., 2016. Icing forecasting for power transmission lines based on a wavelet support vector machine optimized by a quantum fireworks algorithm. Applied Sciences, 6(2), p.54.

Makkonen, L., 1984. Modeling of ice accretion on wires. Journal of Applied Meteorology and Climatology, 23(6), pp.929-939.

Makkonen, L., 1998. Modeling power line icing in freezing precipitation. Atmospheric research, 46(1-2), pp.131-142.

Mittermeier, M., Bresson, E., Paquin, D. and Ludwig, R., 2022. A deep learning approach for the identification of long-duration mixed precipitation in Montréal (Canada). Atmosphere-Ocean, 60(5), pp.554-565.

Niu, D., Wang, H., Chen, H. and Liang, Y., 2017. The general regression neural network based on the fruit fly optimization algorithm and the data inconsistency rate for transmission line icing prediction. Energies, 10(12), p.2066.

Périard, G., 2018. Rapport glacimétrique saison 2018–2019. Rapport interne d'Hydro-Québec.

Rossi, A., Jubayer, C., Koss, H., Arriaga, D. and Hangan, H., 2020. Combined effects of wind and atmospheric icing on overhead transmission lines. Journal of Wind Engineering and Industrial Aerodynamics, 204, p.104271.

Sheng, C., Tang, Q. and Hong, H.P., 2023. Estimating and mapping extreme ice accretion hazard and load due to freezing rain at Canadian sites. International Journal of Disaster Risk Science, 14(1), pp.127-142.

Snaiki, R., 2024. Performance-based ice engineering framework: A data-driven multi-scale approach. Cold Regions Science and Technology, p.104247.

Snaiki, R., Jamali, A., Rahem, A., Shabani, M. and Barjenbruch, B.L., 2024. A metaheuristic-optimization-based neural network for icing prediction on transmission lines. Cold Regions Science and Technology, p.104249.

Sun, W. and Wang, C., 2019. Staged icing forecasting of power transmission lines based on icing cycle and improved extreme learning machine. Journal of cleaner production, 208, pp.1384-1392.

Yip, T.C., 1995. Estimating icing amounts caused by freezing precipitation in Canada. Atmospheric research, 36(3-4), pp.221-232.

Zhang, Z., Huang, H., Jiang, X., Hu, J. and Sun, C., 2012. Analysis of ice growth on different type insulators based on fluid dynamics. Diangong Jishu Xuebao(Transactions of China Electrotechnical Society), 27(10), pp.35-43.

CHAPITRE 4

CONCLUSIONS GÉNÉRALES ET PERSPECTIVES

4.1 Conclusions

Dans ce mémoire de maîtrise, les travaux se sont concentrés sur trois axes principaux.

Le premier axe de recherche, présenté dans l'article 1 au **chapitre 2**, s'est focalisé sur le développement d'un modèle à ordre réduit performant capable de prédire l'évolution temporelle de l'épaisseur de l'accumulation de glace sur les lignes de transmission aériennes, en mettant particulièrement l'accent sur le rapport glace-liquide (ILR). À notre connaissance, aucune étude antérieure n'a proposé un tel modèle intégrant des réseaux de neurones artificiels et des algorithmes d'optimisation métaheuristiques pour atteindre des résultats courageux.

Les deuxième et troisième axe de recherche, présentés dans l'article 2 au **chapitre 3**, se sont concentrés sur l'élaboration de deux types de cartes spécifiques à la région du Québec. À notre connaissance, et selon la littérature existante, aucune étude précédente n'a développé de cartes similaires.

- **Première carte** : des cartes des épaisseurs maximales annuelles de givrage, conçues pour soutenir une planification efficace et résiliente des réseaux électriques.
- **Deuxième carte** : des cartes d'aléas de risques (faible, modéré, élevé), permettant de localiser et de mieux anticiper les impacts des conditions climatiques extrêmes.

Ces cartes ont été créées à partir des données réelles des épaisseurs maximales annuelles de dépôt de glace, mesurées par les stations glacimétriques d'Hydro-Québec. Elles visent à fournir des outils pratiques pour la conception et la gestion des infrastructures face aux défis posés par le changement climatique.

Pour plus de clarté, les principales conclusions de ce mémoire peuvent être résumées comme suit :

1. Développement d'un modèle à ordre réduit pour la prédiction du givre sur les lignes électriques
    a. Le travail a été réalisé en deux phases.
        i. **Première phase** : Une analyse de sensibilité globale a été menée en calculant les indices de Sobol totaux et en les comparant avec la méthode de Monte-Carlo, complétée par les indices totaux de Kucherenko. Cette analyse a révélé que les paramètres les plus influents sur la variance de la sortie du modèle sont les précipitations, la température, la température du point de rosée et la vitesse du vent. Ces variables ont été retenues pour les étapes ultérieures.

ii. **Deuxième phase** : Un modèle basé sur un réseau neuronal à propagation avant (FFNN) a été développé et ensuite optimisé à l'aide de quatre métaheuristiques : PSO, GWO, WOA et SMO. Ces méthodes se sont révélées plus performantes que l'optimisation par descente de gradient stochastique (SGD), avec des valeurs de MSE avoisinant 2.29E-02 et des coefficients de corrélation supérieurs à 0.80. Ces métaheuristiques ont démontré leur efficacité en évitant les optima locaux et en convergeant rapidement vers l'optimum global.

Ce modèle proposé représente une avancée significative pour la prévision du dépôt de verglas, offrant des perspectives prometteuses pour la communauté météorologique.

2. Élaboration de cartes des risques de givrage pour le Québec

Des cartes des risques de givrage ont été développées pour trois périodes de retour : 10, 30 et 50 ans.

Modèle probabiliste : Trois distributions de probabilité (Gumbel, log-normale et GEV) ont été testées. Parmi celles-ci, la distribution de Gumbel s'est avérée la plus adaptée pour représenter les épaisseurs maximales annuelles de givrage à partir des données d'Hydro-Québec.

Interpolation spatiale : Les techniques d'interpolation par pondération inverse à la distance (IDWI) et de krigeage ordinaire ont été utilisées pour produire des cartes offrant une visualisation précise des risques à l'échelle spatiale.

Ces cartes constituent un outil essentiel pour la gestion et la prévention des impacts liés au givrage dans les régions nordiques.

3. En s'appuyant sur le cadre (PBIE), le phénomène de galop, un facteur crucial pour la sécurité des lignes de transmission en conditions sévères de givrage, a été pris en compte. Cela a permis d'élaborer des cartes détaillées des risques associés, pour les mêmes périodes de retour définies dans la deuxième phase du travail, en utilisant les techniques (IDWI) et de krigeage ordinaire.

4.2 Travaux futurs et limitations

Les revues de littérature et les questions explorées dans ce mémoire mettent en évidence l'importance de la relation entre l'accumulation de glace sur les lignes de transmission, la vitesse du vent et l'apparition des tempêtes hivernales, en particulier les tempêtes de verglas. Ce domaine de recherche est très prometteur et offre de nombreuses perspectives pour approfondir la compréhension de deux aspects clés :

1. Amélioration de la prédiction de l'épaisseur de glace lors d'un événement de verglas, afin de mieux anticiper les risques associés.

2. Étude de l'impact de la vitesse du vent sur le déclenchement du phénomène de galop, crucial pour la sécurité des lignes de transmission.

En d'autres termes, il s'agit de savoir comment cartographier efficacement l'épaisseur de givrage pour optimiser la conception des réseaux électriques et évaluer les aléas de risques climatiques.

Dans cette optique, il est recommandé de poursuivre les recherches pour améliorer davantage les résultats obtenus et répondre aux questions soulevées dans ce mémoire.

- Les performances du modèle à ordre réduit, mesurées par l'erreur quadratique moyenne (MSE) et le coefficient de corrélation (R), se sont révélées très satisfaisantes avec l'utilisation d'une seule couche cachée et de quatre métaheuristiques mentionnées précédemment. Toutefois, ce modèle pourrait être davantage optimisé en adoptant un réseau de neurones artificiels de type Perceptron Multicouche (Multilayer Perceptron, MLP) et en explorant d'autres métaheuristiques d'optimisation.
- Les cartes des risques de givrage pour le Québec, développées pour trois périodes de retour (10, 30 et 50 ans), couvrent uniquement une zone géographique limitée. Elles s'appuient sur les données d'une cinquantaine de stations glacimétriques, sans intégrer l'influence de la topographie (altitude). Il est donc recommandé, pour les recherches futures, d'étendre cette couverture à l'ensemble du territoire québécois et de prendre en compte les variations topographiques pour une meilleure précision.
- Les cartes de givrage pour les trois périodes de retour ont montré que les valeurs maximales de givrage se concentrent principalement autour du fleuve Saint-Laurent. Cette observation suggère l'existence de conditions climatiques spécifiques, en complément des facteurs tels que la température, la vitesse du vent et les précipitations, qui pourraient favoriser une accumulation accrue de glace dans cette zone. Une analyse plus approfondie et détaillée de ce phénomène est recommandée pour en clarifier les causes et les mécanismes sous-jacents.

- À l'instar de l'analyse de sensibilité basée sur la méthode du chaos polynômial en expansion (PCE), il serait possible de développer un modèle probabiliste permettant d'analyser les incertitudes associées aux paramètres d'entrée du modèle actuel.